THESIS FOR THE DEGREE OF DOCTOR OF PHILOSOPHY

Damage and defects in railway materials:

Influence of mechanical and thermal damage on crack initiation and propagation

CASEY JESSOP

Department of Industrial and Materials Science

CHALMERS UNIVERSITY OF TECHNOLOGY

Gothenburg, Sweden 2019

Damage and defects in railway materials:

Influence of mechanical and thermal damage on crack initiation and propagation

CASEY JESSOP
ISBN 978-91-7905-132-7

Doktorsavhandlingar vid Chalmers tekniska högskola
Ny serie nr 4599
ISSN 0346-718X

Department of Industrial and Materials Science
Chalmers University of Technology
SE-412 96 Gothenburg
Sweden
Telephone + 46 (0)31-772 1000

Cover: Examples of squats of different severity in field, and an example of spalling (far right).

Chalmers Reproservice
Gothenburg, Sweden 2019

Damage and defects in railway materials

Influence of mechanical and thermal damage on crack initiation and propagation

Casey Jessop

Department of Industrial and Materials Science, Chalmers University of Technology

Abstract

With rising societal concern for the environment, railways offer travelers a sustainable alternative to other forms of fossil-fueled transportation. In order to be competitive with airlines, for example, the railway industry must provide safe, efficient, and affordable service. In the current state, frequent delays on many networks and some rare accidents lead travelers to question the reliability and safety of the rail transport system. This problem is a complex mishmash of different matters which must be addressed from various perspectives. This study focuses on the materials in wheels and rails themselves.

Railway wheel and rail materials are subjected to extreme stress in the field; increasing speeds, loads, traffic, at times in harsh weather conditions aggravate this. The combination of loadings affects the materials in a multitude of ways, for example through mechanical and thermal damage. One of the most common types of mechanical damage in the railway industry is rolling contact fatigue (RCF), the effect of which is frequently manifested in the surface of railway components, as cracks. Thermal damage, on the other hand, can affect both the surface and bulk of the material.

The aim of this project is to properly characterize mechanical and thermal defects in railway components, and evaluate their effects on crack initiation and propagation, and on mechanical properties. This has been approached through extensive characterization of field samples with a certain type of cracks called squat cracks, which in some cases may lead to rail break. The squat crack networks were examined through a variety of methods, followed by the recreation of similar defects in the laboratory. Finally the effect of such defects on the microstructure, crack initiation and propagation in laboratory experiments was evaluated.

Squat crack networks were characterized using several methods; detection limits of each technique have been clarified, and it was concluded that using a combination of methods, the network can be accurately described on many scales. In a second part, well-defined thermal damage on rail surfaces called white etching layers (WELs) similar to those found in field were produced using laser welding equipment, and the effect of these WEL spots on crack initiation and fatigue life has been shown. The WELs reduce fatigue life by providing a crack initiation site; both by stress and strain concentration and by decreasing ductility. The effect of thermal damage on bulk properties was also investigated using microscopy techniques including electron backscatter diffraction (EBSD) and differential-aperture X-ray microscopy (DAXM). It was found that the variation in local misorientation and residual strains decrease with increasing annealing temperature. Additionally, a method to examine crack face friction has been identified, and using this method, similar crack face features to those observed in cracks from field are created in the lab. The results from the friction experiments can be used as input towards crack propagation experiments.

to all the boys i've loved before

Preface

This thesis is based on the work performed in the Department of Industrial and Materials Science between March 2014 and June 2019. The project has been carried out under the supervision of Professor Johan Ahlström, and with Professor Christer Persson as examiner.

This work has been a part of research activities within the Centre of Excellence CHARMEC (Chalmers Railway Mechanics). It is partly financed within the European Horizon 2020 Joint Technology Initiative Shift2Rail through contract No. 730841, as well as partly in the project In2Track2 under grant agreement No 826255.

The authors acknowledge additional support from:

- Vinnova verification for growth programme;
- MAX4ESSFUN;
- InterReg.

Acknowledgements

First and foremost, I would like to thank my supervisor Johan Ahlström for all the amazing help and support in the last 5+ years it took me to finish. Thanks also to all my colleagues and friends throughout the years at MoT/IMS and CHARMEC, and a special shout-out goes out to Monkey Club and NSYNC for sticking around for better, for worse, in sickness and in health... And most of all, thanks to my family in Montréal, I love you more than anything. Vous êtes ma vie, without you I am nothing ♥ ♥ ♥

Thesis

The thesis consists of an extended summary and the following appended papers:

Paper 1: 3D characterization of rolling contact fatigue crack networks

C. Jessop, J. Ahlström, L. Hammar, S. Fæster, and H. K. Danielsen, *Wear*, vol. 366–367, pp. 392–400, 2016.

Paper 2: Crack formation in pearlitic rail steel under uniaxial loading: effect of initial thermal damage

C. Jessop, J. Ahlström, in *LCF8 Eighth International Conference on Low Cycle Fatigue*, 2017, pp. 275–280.

Paper 3: Damage evolution around white etching layer during uniaxial loading

C. Jessop, J. Ahlström, C. Persson, Y.B. Zhang, *Fatigue & Fracture of Engineering Materials & Structures,* 2019, *Article in press* (doi:10.1111/ffe.13044)

Paper 4: Friction between pearlitic steel surfaces

C. Jessop, J. Ahlström, *Under review for international publication*

Paper 5: Effect of annealing on microstructure and strain in railway wheel steel characterized by electron and synchrotron X-ray diffraction

C. Jessop, Y.B. Zhang, D. Nikas, J. Ahlström, *In manuscript*

Not appended:

Friction between pearlitic steel surfaces

C. Jessop, J. Ahlström, 11th International Conference on Contact Mechanics and Wear of Rail/Wheel Systems, The Netherlands, 2018.

The appended papers have been prepared in collaboration with the co-authors. The author of this thesis was the main responsible for the progress of the work, i.e. took part in planning the papers, carried out the majority of experiments, analyzed the results and wrote the major part of the papers. In Paper 1, the radiography and image processing was done by L. Hammar, and the tomography experiments and analysis were done by S. Fæster. The tomography experiments and analysis in Paper 3 were done by Y.B. Zhang. In Paper 5, the experimental work for was done in collaboration with the co-authors: Y.B. Zhang performed the DAXM experiments, and D. Nikas performed the SEM and EBSD experiments. The results processing was done with their help.

Contents

Introduction

Damage in rail materials is both an economic and a safety concern. Regular maintenance and correct characterization of defects in field help reduce predictable rail failures. However, there is real danger when damage and service-induced defects form during extreme circumstances. Some special events lead to elevated loading conditions and/or decreased resistance of the components to damage. In such cases, larger cracks can form and lead to unplanned replacements, costly maintenance, delays, and increased risks for failure, all of which lead to reduced reliability of the system.

Although railways remain a safer alternative than roads when it comes to the number and severity of accidents that occur every year, some incidents involving trains cause people to lose confidence in the railway system and opt for cars and other means of transportation instead [1]. According to Allianz pro Schiene, based in Germany, the number of deaths per billion passenger–km is orders of magnitude smaller than those occurring in cars and even buses, at only 0.01 versus 2.77 and 0.16, respectively [2]. It is important to maintain the integrity of railways, and safety is a major concern for the current industry, with several accidents causing widespread recognition of the damage present. For example, in October 2000, a derailment in Hatfield, England that caused four fatalities raised awareness of the importance of maintaining railways for the British railway industry. The Hatfield accident was the result of overlooked severity of RCF in the rails, with inadequate or neglected maintenance being a main cause [3]–[5].

There are many benefits to be gained from researching railway materials. Railway transport has the lowest CO_2 emissions, based on the 2010 International Transport Forum on Greenhouse Gas Emissions, making it an environmentally conscious form of transportation when compared with road and domestic aviation [2]. While road accounted for 72 % of transport CO_2 emissions in 2008, and domestic aviation for 5 %, rail transport only represented 2 %, with 2.7 billion passenger-kilometers and over one million kilometers of lines worldwide [2]. There are many advantages of railways as a means of freight and passenger transport, and the research undertaken worldwide aims to further improve the environmental, safety, and economic aspects.

Rolling contact fatigue (RCF) has greatly been over-looked in the past, however some accidents raised awareness of the severity of these defect types, and the importance of proper maintenance of railway infrastructure. Replacing rails is expensive, and in order to decrease these costs while assuring safe and secure transportation, judging the severity of damage is of primary importance. This includes a good understanding of the mechanisms of crack initiation and propagation, and associate these to the current state of damage and defects present. Early detection of RCF surface and near-surface defects could help reduce the frequency and intensity of failures and accidents. In order to develop a proper maintenance system, first it is important to understand the nature, cause, and consequences of different types of defects.

The aim of the project has been to properly characterize mechanical and thermal defects in railway components, and evaluate their effects on crack initiation and propagation, and on mechanical properties. This includes evaluating the influence of initial damage, climatic conditions, and material properties. In this study, the aim was achieved through in-depth characterization of a few selected squats and RCF cracks from field samples. Next, fatigue tests were performed to investigate the effect of initial thermal damage on crack initiation. The effect of temperature on the microstructure degradation has also been evaluated through different methods. Furthermore, the influence of different climatic conditions on the crack propagation was investigated. The results serve as necessary input for suitable models for crack initiation and propagation within parallel CHARMEC projects.

Background

Rolling Contact Fatigue

Railway transport offers many benefits to both passengers and freight transport, however proper maintenance and knowledge of the material properties are important for reliable operation. The damage to the metal components, wheels, and rails, is related to the wear and tear of the materials themselves from the regular train operations. The main concern is not the normal use, but rather when unpredicted failures occur due to failure of the materials, for example rail breaks or derailments.

Rolling contact fatigue (RCF) is a major concern for the railway industry today as one of the main causes of component failure following increased traffic, accelerations, and loading conditions. The wheel/rail contact condition that occurs in railway applications is complex, and it is essential to understand the associated damage from combined mechanical and thermal loadings in order to predict component life and develop appropriate maintenance systems. The crack initiation and propagation processes of RCF have been extensively studied from both theoretical and experimental points of view [6]–[14]; however, certain mechanisms for crack initiation and propagation are still not well understood. Thermally damaged surface layers, often called white etching layers (WELs), seem to contribute to crack initiation [15]–[19]. One hypothesis is that cracks nucleating in or close to WELs can develop into so-called squats or studs in the rail, and to RCF clusters in wheels.

Rolling contact fatigue cracks

Rolling contact fatigue (RCF) is defined as the fatigue of materials in contact in conjunction with rolling contact and normal loads. A commonly occurring form of RCF cracking is head checks (Figure 2). These are recurring cracks on the gauge corner of rails, but are benign and usually removed by regular rail grinding and maintenance [20]–[22]. However, if not properly maintained, gauge corner cracking (GCC) can lead to the formation of squat cracks. In recent years, the occurrence of this type of surface-initiated defect has been more present and studied. These squats and squat type defects can be a problem due to their location in the rail. Depending on the loading scenario and the orientation of the crack tip, they can either plateau parallel to the surface, or they can turn downwards and cause complete rail fracture.

Fatigue occurs due to the repeated rolling contact between the wheels and rails combined with extreme loads in a very small contact patch on the material in both rail components. This loading causes large stresses within the components, which lead to severe plastic deformation of the topmost layer of the material when the cyclic yield limit in shear is repeatedly exceeded for thousands of cycles [23]–[26]. Cracking and increased risk of fracture may occur as a result.

Different types of loading conditions in service result in different RCF defect types, some examples are shown schematically in Figure 1 [12]. These depend on the location of the contact patch between the wheel and the rail as well as the contact condition, both of which vary with profile changes of the components. Subsurface cracks can form within the bulk of the material, for example on the left, or cracks can initiate for surface irregularities and propagate into the material at a shallow angle, as shown in the middle.

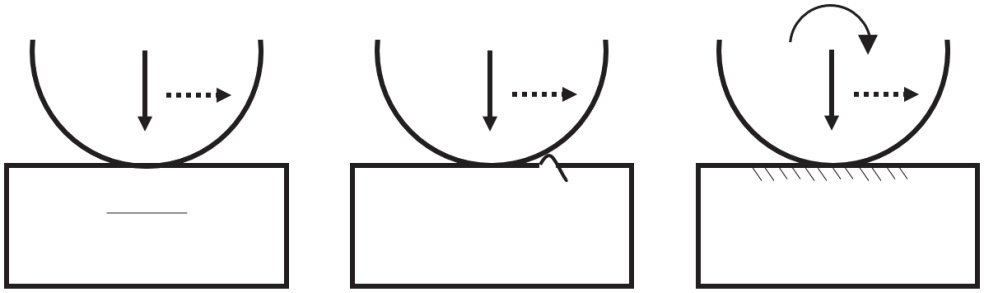

Figure 1. Different types of contact loading and the resulting crack formation. Modified from [12]. [27]

In the last few decades, awareness of so-called "squats" has increased due to higher occurrence of this type of service-induced defect [6], [8], [19], [28]–[30]. Some examples of squats are shown in Figure 3. The name originated from the apparent shape of the crack formation on the surface of the rail, which looks as though a heavy gnome squatted on the rail, leaving an indentation of two lobes of similar size [31]. The two-lobe form on the surface of a rail suggests a planar crack network below the surface, causing internal wear within the crack. This in turn causes the rail surface to sink and take on a darker appearance due to less surface wear. Metallographic cross-sectioning shows an initial crack growing at small angles, around 10° to 30°, from the surface of the rail and then deviating to propagate nearly parallel to the surface within a shallow depth (typically less than 5 mm) [17], [19], [32]. Head checks, such as those shown in Figure 2, occur on the gauge corner of high rails in shallow curves [33]. Generally this type of RCF defect is not a cause for major concern, since a combination of wear and regular maintenance grinding removes the thin layer in which the cracks are present. In some cases, such as those shown schematically in Figure 4, the cracks can branch upwards towards the surface as it progresses [34], causing spalling (far-right image in Figure 3 and Figure 4b), which leads to increased impact loading on further traffic. The crack growth can also deviate into a downwards angle, leading to increased risk of rail break (Figure 4c) [13].

Figure 2. Commonly occurring RCF defects on the gauge corner of rails. Dashed lines highlight the curvature of the head checks from the gauge corner into the running band. [27]

Squats are surface- or near-surface-initiated defects, thought to originate due to local plastic deformation of the surface as a result of RCF loading, including dynamic wheel/rail contact forces [11], [13]. Some types of squats, in which local thermal damage to the rail surface affects the initiation mechanism, are often referred to as studs [11], [35]. However, it should be noted that the distinction between squats and studs is not always made [13], [28], [36]–[40]. A stud (squat-type defect) is not formed due to severe plastic deformation of the surface pearlite layer, but develops in less deformed pearlite and propagates through grains [35].

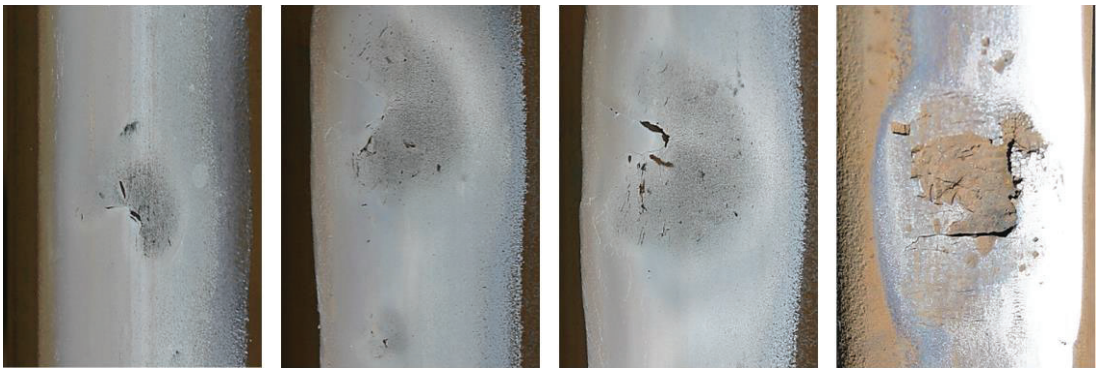

Figure 3. Examples of squats of different severity in field, as well as an example of spalling (far right). [27]

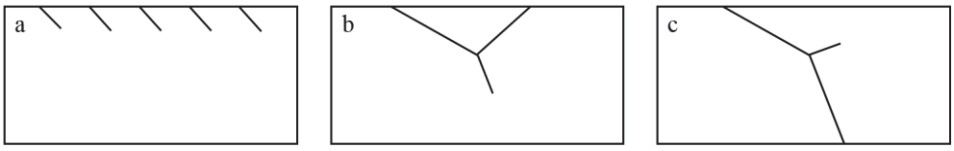

Figure 4. Schematic showing three levels of severity of RCF cracks on rail surface: (a) small cracks, (b) spalling, and (c) risk for rail break. (Longitudinal section) [27]

Crack initiation from thermal damage

In addition to mechanical damage, the rails and wheels are subject to thermal damage, which can have an effect on RCF crack formation [17], [19]. Rapid heating followed by rapid cooling of a thin layer of material on the surface of the rails and wheels (for example, due to wheels slipping during braking, accelerating) can cause martensite to form. When the temperature at the wheel/rail contact exceeds the effective austenitization temperature (roughly 800 °C [41]), phase transformation to austenite occurs. The thin layer transformed is then rapidly cooled by heat conduction into the cool surroundings. The thin martensite layer forming on cooling is referred to as white etching layer (WEL) due to the white, featureless appearance under optical microscopy after etching (Figure 5) [42], [43]. These WELs have different properties compared to the bulk pearlitic material, and therefore can promote crack initiation as well as spalling. The hard and brittle martensite is more prone to cracking compared to the bulk, which is more ductile. Crack initiation related to WELs is a common problem in the railway industry that is observed in both rails and wheels [11], [24], [42]–[44]. Figure 5 shows two typical types of cracks related to WEL, that is, those that grow at the interface of the WEL and the bulk material (Figure 5a), and those that grow through the WEL (Figure 5b).

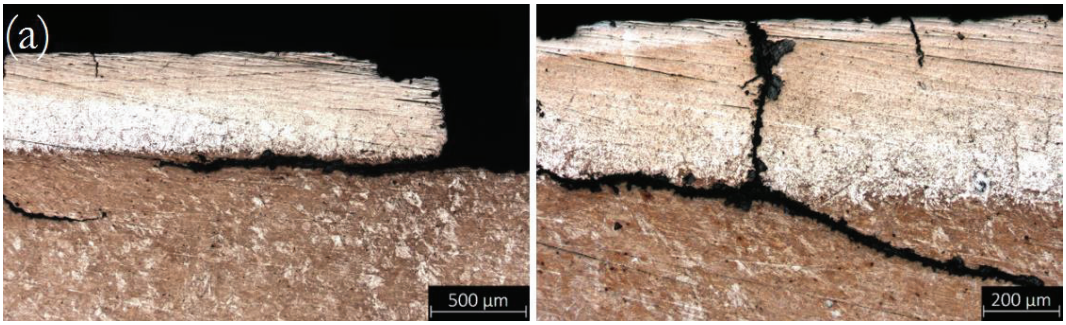

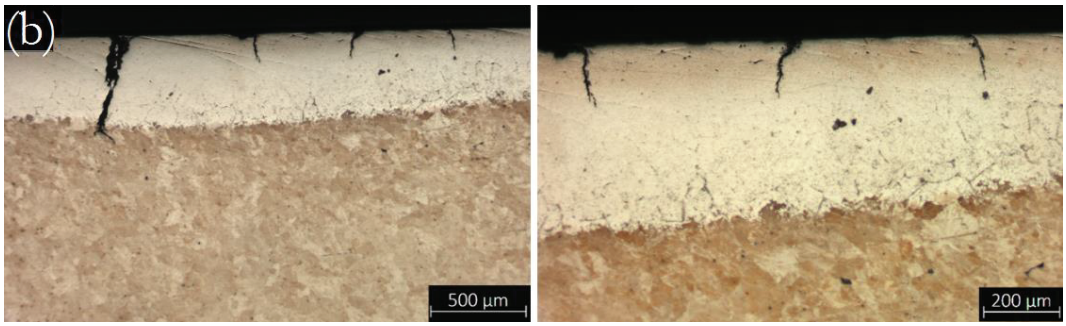

Figure 5. (a) Cracks growing at interface of WEL and bulk, and (b) growing through WEL. [45]

The formation of WELs also introduce residual stresses in rails, which are due to the changes in volume from thermal expansion on local heating, leading to plastic deformation at high temperature, and volume expansion on phase transformation from pearlite via austenite to martensite. The presence of these residual stressed also increases the risk of crack initiation around these thermally affected areas [27], [46]. Residual stresses will be discussed in more detail the next section.

The previously described defects are more frequent in the rail material, however in the wheels, the thermal damage can also affect the bulk more severely. Wheel steel has a slightly different composition than rail steel, but remains pearlitic steel, with a portion of free ferrite in between the pearlitic colonies (see Figure 6a and Table 1). Due to the longer duration of heating in the wheels, the increased temperature can affect the mechanical properties and the microstructure of the bulk [47], [48]. The manufacturing processing of wheels introduces residual stresses in the material which are favourable for preventing fatigue cracking from the wheel running surface. Some of these residual stresses are released during a final annealing step in the process. However the thermal damage occurring, for example, during block braking in freight wheels, exposes the material elevated temperatures up to 550 °C during long-duration drag braking [49]. The effect of similar temperature events on the mechanical properties of the wheel are of significant interest when studying the damage and defects present in these components.

Frequent heating can lead to cracking, but also degradation of the material, and in turn the mechanical properties can deteriorate [48], [50]. One phenomenon which is observed is spheroidization of the pearlitic structure in wheel steel, an extreme example of which is seen in Figure 6b. The effect of this degradation has an impact on both the mechanical properties of the material as well as the fatigue of the component [48], [51].

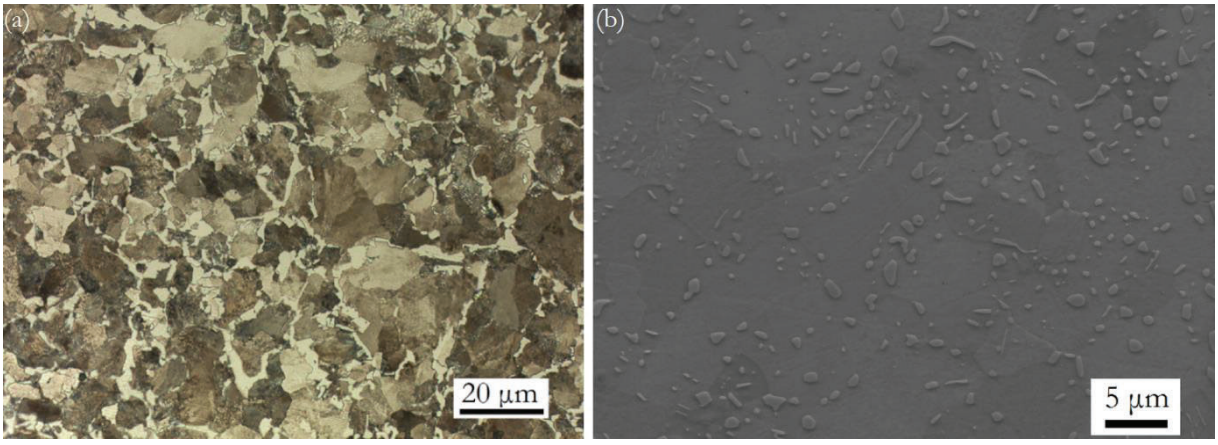

Figure 6. (a) Microstructure of R8T wheel steel, and (b) SEM micrograph of spheroidized microstructure.

Residual stresses

During operation, the application of loads in conjunction with rolling of the wheels on the rails introduce stresses of magnitudes enough to plasticize the material; the stresses that remain in the material after the load is removed are referred to as residual stresses. These stresses are calculated from elastic strains within the crystal lattice. The presence of residual stresses can have positive or negative effects on fatigue life and crack growth rates, depending on their magnitude and whether they are compressive or tensile. While compressive residual stresses tend to hinder crack growth, tensile stresses can increase rates of crack propagation [52].

X-ray diffraction (XRD) is an analysis method that provides information on the atomic and molecular structures of crystalline materials. This technique makes it possible to identify the diffraction peaks of crystalline phases of an investigated sample. It can therefore be used for residual stress measurements by comparing the measured peaks to those of a stress-free specimen.

The principle of the technique is based on X-ray diffraction linked with elastic scattering of electrons, and the high-energy electromagnetic radiation of X-rays. The diffraction mechanism consists of an incoming X-ray wave, initially confined to a single direction, which interacts with the crystals in a sample and diffracts in different directions depending on the symmetry of the unit cell. This interference is shown schematically in Figure 7, and follows Bragg's law:

$$n\lambda = 2dsin\theta$$

Where n is an integer value, λ is the wavelength of the incident wave, d is the inter-planar spacing, and θ is the angle between the incident X-ray and the atomic plane [53]. In steels, the sampling depth of diffracted X-rays from laboratory instruments is limited to approximately 5 μm below the surface.

A peak shift in the diffraction pattern indicates a strain in the material caused by an increase or decrease (elongations or contractions) of the inter-planar spacing in the crystal lattice. The measurement of residual stresses is calculated assuming a plane stress state; that is, the stress normal to the surface is zero [54].

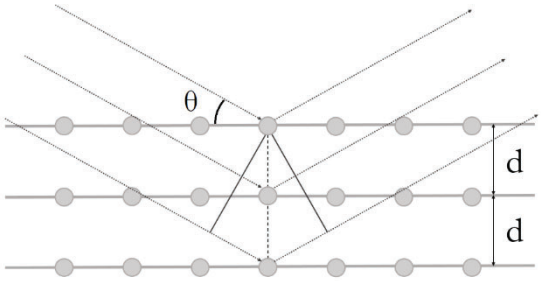

Figure 7. X-ray diffraction; d is the spacing between the atomic planes, and θ is the angle between the incident X-ray and the atomic plane.

The strains can be calculated in terms of inter-planar spacing using the aforementioned set-up, but it is more useful to know the residual stresses in the sample. The $\sin^2\psi$ method is the technique most commonly used for residual stress analysis. The measurements taken at chosen $\sin^2\psi$ angles are plotted against the inter-planar spacing, and the stress can be determined from the following relation [54]:

$$\sigma_\varphi = \frac{E}{1+\nu} m$$

Where E is Young's modulus, ν is Poisson's ratio, and m is the gradient of the d versus $\sin^2\psi$ curve.

Fatigue testing

Low-cycle fatigue

The low-cycle fatigue (LCF) life of a material is characterized by the strain-life (Coffin-Manson) curve, a log-log plot of the plastic strain amplitude versus number of cycles to failure, according to the following equation [55]:

$$\varepsilon_{\mathrm{pa}} = \varepsilon_{\mathrm{f}}'(2N_{\mathrm{f}})^{c}$$

Where ε_{ea} is the plastic strain amplitude, ε_f' is the fatigue ductility coefficient, N_f is the number of cycles to failure ($2N_f$ is the number of reversals to failure), and c is the fatigue ductility exponent. ε_f' and c are considered material properties [56].

For strain-controlled fatigue tests, which are commonly used for LCF, the specimen is cycled between a maximum and minimum strain, and the stress response is measured. The relationship between the stress and strain at each cycle is presented in the form of a hysteresis loop (an example is shown in Figure 8). The Bauschinger effect is evident in the first cycle, i.e. after the first tension loading, the material yields at lower stress upon reversed loading. There is typically an initial transient in the stress amplitude, but after some cycles the behavior stabilizes and the stress amplitude varies less until larger cracks develop, resulting in a decreased peak stress level. Eventually, cracks grow to cause failure of the specimen.

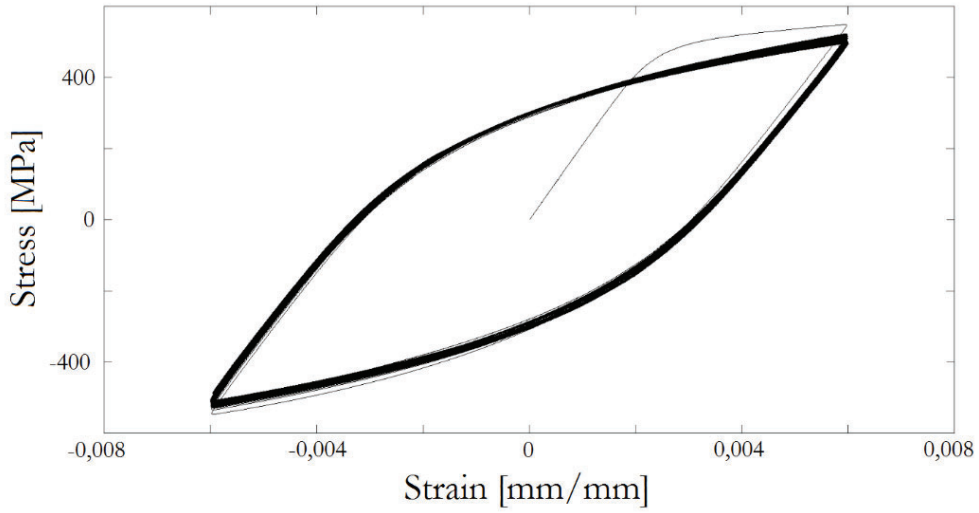

Figure 8. Typical hysteresis loops for strain-controlled LCF test in uniaxial cyclic loading, with constant total strain amplitude of 0.6 % in this case. The stress amplitude registered in this case decreases throughout the test.

Surface initiated rolling contact fatigue

The study of fatigue in a material can be approached from two perspectives: a fatigue damage approach, or a fracture mechanics approach, when cracks are explicitly defined in a given model. In the current work, only fatigue damage is considered, which includes input from operating conditions and subsequent damage in terms of plastic deformation or thermal damage, as previously discussed. The contact occurring between the wheel and rail is generally described using Hertzian theory [57], which defines an elliptical contact area, with semi-axes in the rolling (x) and lateral (y) directions. The size and shape of the contact depends on the normal force and the rolling direction [12], [23].

The magnitude of the maximum contact pressure, p_0, occurring at the center of the ellipse, is:

$$p_0 = \frac{3F_z}{2\pi ab}$$

Where F_z is the load in the z-direction. One assumption which can be made is full-slip in the contact area, in which case the shear stress, or traction, will be proportional to the contact pressure. Therefore, the peak traction, q_0, is defined as:

$$q_o = f \cdot p_0$$

Where f is the traction coefficient. Furthermore, if the material yield limit in cyclic shear, k, is reached, then surface plasticity will occur, and can be expressed as:

$$q_0 = k$$

or

$$f \cdot p_0 = k$$

The shakedown map is used to define the fatigue damage in a given contact patch, based on the normalized vertical load and the traction coefficient. That is, the risk of surface of subsurface RCF crack initiation and growth can be determined based on the region associated to the operating conditions [12], [58].

Experimental methods

Materials

The materials studied in the thesis are pearlitic steels with slightly different compositions and properties which are used for rails (R260) and wheels (R8T). The compositions are summarized in Table 1.

Table 1. Composition of rail and wheel steels (in wt. %).

	C	Mn	P	S	Cr	Si	Mo	Ni	V	Fe
R260	0.72	1.04	0.006	0.010	0.02	0.31	-	-	-	Bal.
R8T	0.59	0.78	0.005	0.006	0.13	-	0.05	0.17	<0.005	Bal.

Characterization of RCF damage and defects

The characterization of defects found in rails and wheels can be done on a variety of scales using many different methods. Within this project, several methods were used to examine rail sections taken from the field down to single ferrite grains within wheel steel. The following chapter will briefly summarize the methods used in the appended papers.

Microscopy

Microstructural evaluation allows for the material microstructure and mechanical properties to be compared. Sample preparation for evaluation under microscopy includes surface finishing (grinding and polishing) and etching, which are done according to the specimen and to the purpose of the investigation. All grinding and polishing was done using Struers preparation equipment, and etching with Nital (2-3 % HNO_3 in ethanol) for different amounts of time. Investigations were carried out using a Leitz DMRX optical microscope, a Zeiss SteREO Discovery V20 stereomicroscope, and a LEO 1450VP SEM scanning electron microscope (SEM). Optical microscopy allows for an overview of the microstructure including the different phases present, including for example the deformation and orientation of pearlite colonies. Stereomicroscopy allows for inspection of rough surfaces at lower magnification. However, the depth of focus is not sufficient to obtain clear images of a textured surface, which requires the use of SEM. Using SEM, better spatial resolution, depth of focus, and higher magnification are achieved.

Topography measurements

A Somicronic Surfascan 3D stylus-based surface profiler was used to obtain 3D mapping of regions of interest on different specimens. The profiler was fitted with a ST027 stylus probe (2 mm tip radius and a 90° tip angle) and a depth description was acquired. The step size used is decided based on the focus of the measurement. For example, an overall geometrical description was obtained using 1mm step size, while detail maps were done on smaller regions with step size 50 μm [59].

X-ray tomography

X-ray tomography is a non-destructive method which allows for high-resolution 3D visualization of internal features, which has been done using a Zeiss Xradia 520 Versa instrument. For the purpose of the measurements in Paper 1, for example, the X-ray energy was polychromatic up to 160 kV from a tungsten target and 1601 projections of each region were acquired. 3D density maps were reconstructed by a standard

filtered back-projection method to 2k x 2k x 2k pixel volumes with a voxel size of 7.29 μm. More details about the setting of the measurements can be found in the appended papers [45], [59].

Electron backscatter diffraction

The EBSD measurements were carried out in a LEO 1550 high resolution field emission scanning electron microscope (FEG-SEM). The system was equipped with an EBSD detector (Nordlys, Oxford instruments), a high speed camera for EBSD pattern recording, and software for crystal orientation mapping (AZtecHKL). The samples were tilted to 70° and the SEM was operating at an accelerating voltage of 20 kV. Crystallographic orientation maps are taken on the surface of the samples.

Differential-aperture X-ray microscopy

DAXM experiments were conducted at beam line 34-ID-E at the Advanced Photon Source (APS), Argonne National Laboratory. First, a focused polychromatic micro beam (with size of ~0.5 μm) was used to determine the orientations of the grains. The X-ray micro beam scans the sample which is mounted on a holder at an inclination of 45º to the incoming beam. A panel detector mounted in 90º reflection geometry 510.3 mm above the specimen was used to record the Laue diffraction patterns. A Pt-wire of 100 μm diameter, scanning along the sample surface at a distance of 250 μm, was used as a differential aperture for resolving diffraction patterns from different depths penetrated by the micro beam. The Laue patterns at each depth were reconstructed and indexed using the LaueGo software available at beamline 34-ID-E. The crystallographic microstructure within an area of 80-120 μm along the horizontal direction and 100 μm along the depth was mapped for each sample.

A monochromatic beam was then used for measurements of elastic strain within selected grains. By scanning the X-ray energy around the calculated value (calculated from the indexed Laue pattern) for a selected Laue diffraction spot, the intensity distribution as a function of the diffraction vector $Q = 2\pi/d$ (Q-distribution) can be determined for the selected diffraction spot at different depths. At each depth, the Q-distribution is fitted using a Gaussian function and the center of the distribution, Q_C, is used to determine the absolute lattice spacing, *d*. The elastic strain, ε, can then be determined using:

$$\varepsilon = \frac{(d - d_0)}{d_0}$$

where d_0 is the lattice spacing of the sample in the stress-free state. For the present study, d_0 was calculated, according to the chemical composition in Table 1 with lattice parameter a_0=2.86734 Å. More detailed information can be found in [60], [61].

Fatigue testing

The fatigue behavior of the rail steel, as well as the effect of initial thermal damage, was tested using uniaxial strain-controlled fatigue tests at room temperature, at constant total strain rate of 10^{-2} s^{-1}, and at three constant strain amplitudes: 0.4 %, 0.6 %, and 1.0 %. Test bars were machined, ground and polished before testing. Two different conditions were tested: un-notched and with initial thermal damage, Figure 9. The un-notched specimens were tested to provide a basis for fatigue behavior of the material. The thermal damage was in the form of a WEL spot with thickness close to 200 μm, which is a thickness occasionally found in field.

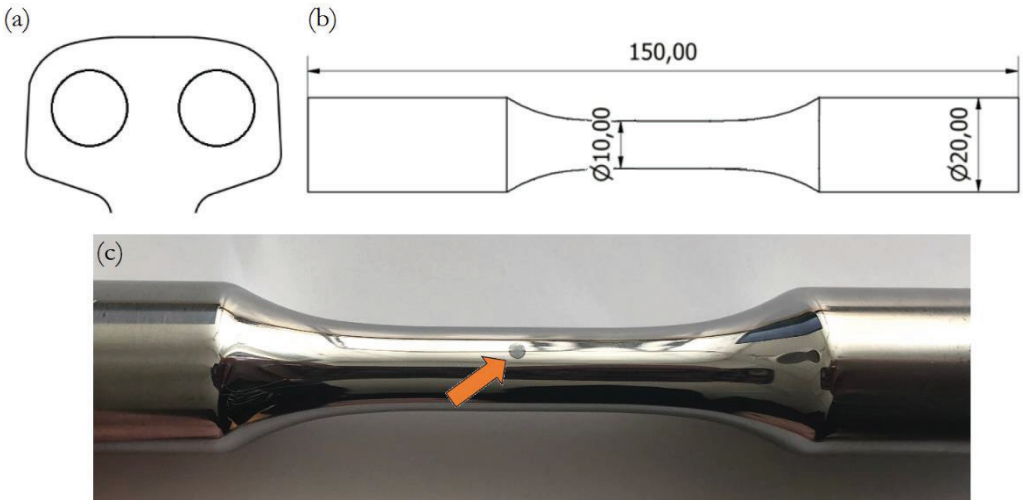

Figure 9. (a) Approximate extraction location of test bars in railhead, (b) specimen geometry, and (c) initial thermal damage (WEL) on polished test bar.

Laser heating experiments

WELs on the surface of rails and wheels are a suspected initiation site for severe RCF cracking [5], [6]. In order to determine the effect of this type of thermal damage on crack initiation and fatigue life, WELs were artificially made on pearlitic rail test bars to be used for fatigue experiments. Furthermore, WELs were made on the running band of new and used rail sections for characterization and comparison. The used rail sections also had white etching layers from operation, which were used for comparison with the artificially produced ones. The laser experiments were performed at Trumpf GmbH, Ditzingen, Germany using a TruDiode laser. The laser beam was tuned to illuminate diameters of 2 mm and 6 mm on the surface of the test bars and rail sections, respectively, and the power was controlled according to different energy pulse shapes. More details can be found in [62].

Digital image correlation

An ARAMIS 3D motion and deformation sensor system, based on digital image correlation (DIC), is used to visually capture the strain evolution on surfaces during experiments. The technique is based on tracking the deformation in the test specimen by comparing images at a given interval to a reference image. The strain field is deduced from the analysis of the displacement field of the specific details painted onto the surface. The specimen is spray painted to obtain a uniform and random speckle pattern on the surface. In the experiments described in Paper 3, the camera was focused on the center of the test bar where the WEL spot was present. Due to the different flow stresses, it can be predicted that the WEL spot will act as a stress-raiser during uniaxial loading, and this will affect plastic strain initiation and accumulation. A snapshot was taken at the maximum load in tension for each cycle.

Residual stress measurements

Residual stress measurements within the project were done using a Stresstech Xstress 3000 X-ray machine with the sin2ψ method and Cr Kα-radiation, with 1 mm or 3 mm collimators used for measurements on test bars with and without initial thermal damage, as well as surfaces of rails taken from the field. The detectors are positioned at $2\theta \approx 156°$ [54]. The measurements were run with the inclination angle ψ between -45° and +45°, using nine equal steps in sin2ψ (i.e. 0°, ±21°, ±30°, ±38°, ±45°), and in 3 directions (Φ=0°, 45°, and 90°).

Crack face friction experiments

Crack propagation is affected by many factors, one of which is crack face friction. The effect of crack face friction is difficult to study, since during crack propagation experiments, the cracks remain tightly closed, and there is no direct way of measuring the friction between the crack faces. Furthermore, the presence of different third-body materials (including wear products, water, lubricants, etc.) is not constant, and has an influence on the friction coefficient. As a starting point to studying the effect of crack face friction on crack propagation, a series of experiments was designed, in which the coefficient of friction would be the focus.

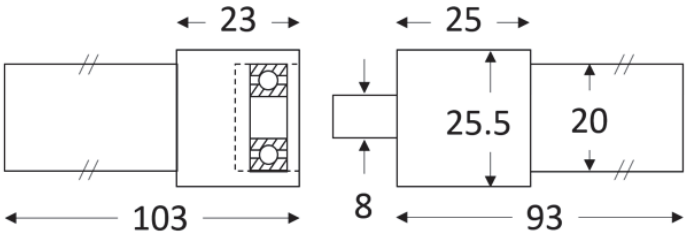

Figure 10. Schematic of test bar used in friction experiments with dimensions in mm.

Using an MTS 809 axial-torsion servo-hydraulic test machine, the two halves of the test bar (shown schematically in Figure 10) were pressed together with varying normal force, sliding velocity (rate of rotation), and angles of rotation (stroke/length of sliding movement), in wet and dry conditions. The friction is determined by the torque required to rotate the sample under a given normal force, according to:

$$\mu = T/F \cdot r$$

Where T is torque [kN·mm], F is the normal force [kN], and r is the average radius in the contact [mm] [63].

Summary of results

Part 1: Characterization of RCF crack networks (Paper 1 and unpublished)

One objective of the work presented in this thesis was to properly describe the three-dimensional geometry of RCF crack networks in rails using several characterization technique. The RCF damage in the wheel and rail sections taken from the field was examined using serial sectioning techniques with optical microscopy (OM), and scanning electron microscopy (SEM). In Paper 1, the following methods were used: high-intensity X-ray radiography complemented with geometrical reconstruction, serial sectioning and metallography in combination with microscopy, X-ray tomography, and topography measurements. The experiments were performed on different squats from rail sections taken from the field.

Using a combination of radiography and geometric reconstruction, a squat crack network was reconstructed and compared to the interpolated network obtained from metallographic sectioning (Figure 11) using MATLAB [64]. The geometry is similar to that described in literature [65]. From this, it can be seen that although the overall geometry is well determined from the geometric reconstruction, certain limitations remain, namely in locating the surface-breaking part of the crack and well as the crack tip depth and orientation. The crack tip is, in fact, perhaps the most important point when looking to determine the severity of a crack in field, since the orientation could determine whether the crack will plateau or will turn downwards and potentially cause rail fracture.

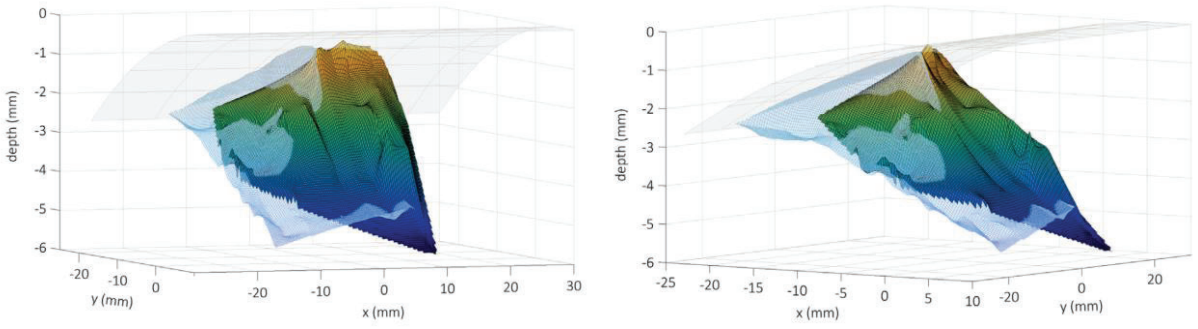

Figure 11. 3D plots with surfaces obtained from both 3D reconstruction (colored) and metallography (mesh). The crack network is showed relative to the rail surface (gray). [59]

A different squat was broken apart and observed under stereomicroscopy to examine features about the crack morphology and topography, shown in Figure 12. Some observed features were further investigated using topography measurements, as shown in Figure 13. This method allowed for an accurate overall description of the main crack using 1 mm step size, and of the ridges using 50 µm step size.

Additional investigation with SEM revealed crack branching in the transverse sections (e.g. Figure 14); while the longitudinal sections provide additional information about the crack geometry below the surface. Figure 13 shows undulations near the end of the crack network as compared to the detail maps. Furthermore, the 3D mapping (Figure 13b) shows a highly textured surface on different scales: some beach marks, ridges, and surface roughness. It can be speculated that the ridges on the fracture surface (Figure 12b) are a result of repeated relative movement of the two crack surfaces in the same direction, while the smoother regions observed near the surface-breaking part of the crack (Figure 12a, top) are a result of rubbing of crack faces in different directions due to an additional shear displacement. This is thought to be a result of the stresses propagating the crack [35].

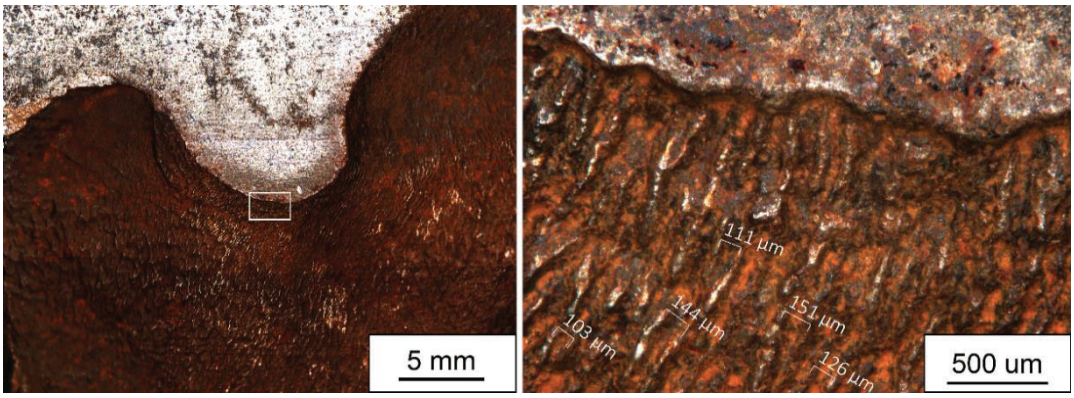

Figure 12. Images from stereomicroscopy of (left) squat surface, and (right) detail close to the tip of the v. [27]

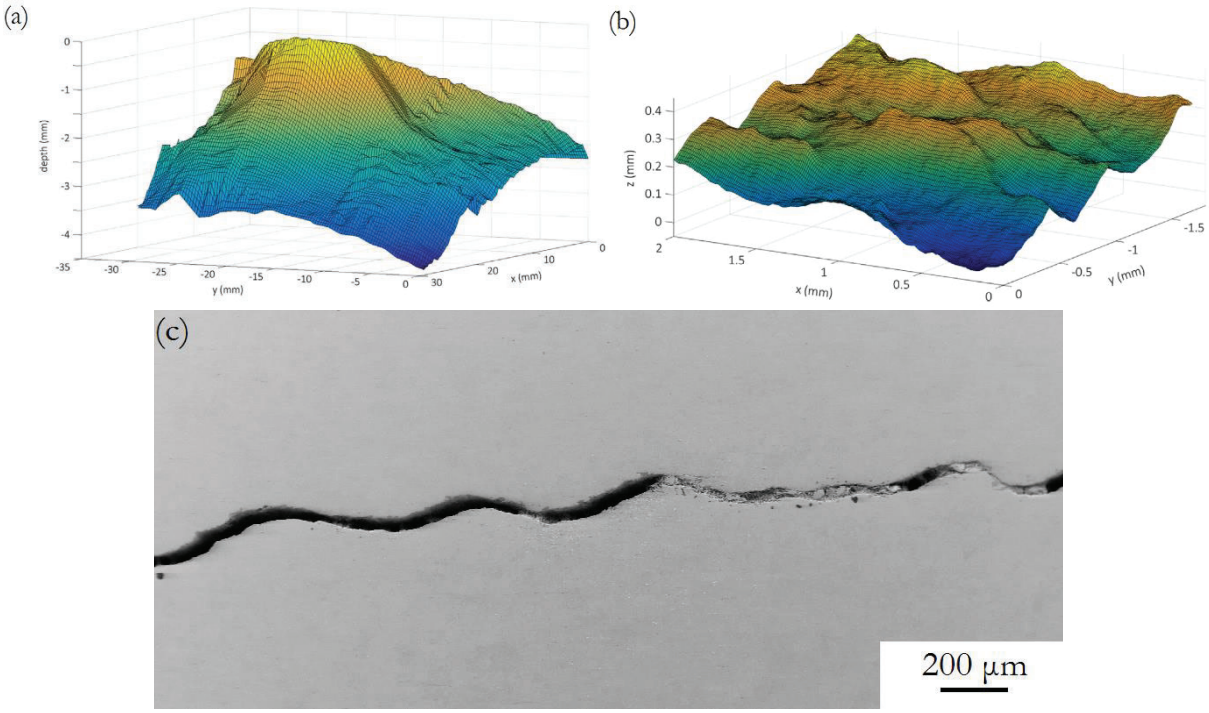

Figure 13. (a) Mapping of overall squat geometry, 1 mm step size. (b) Mapping from topography showing ridges, 50 µm step size. [59] (c) Undulations in longitudinal section of squat network. [27]

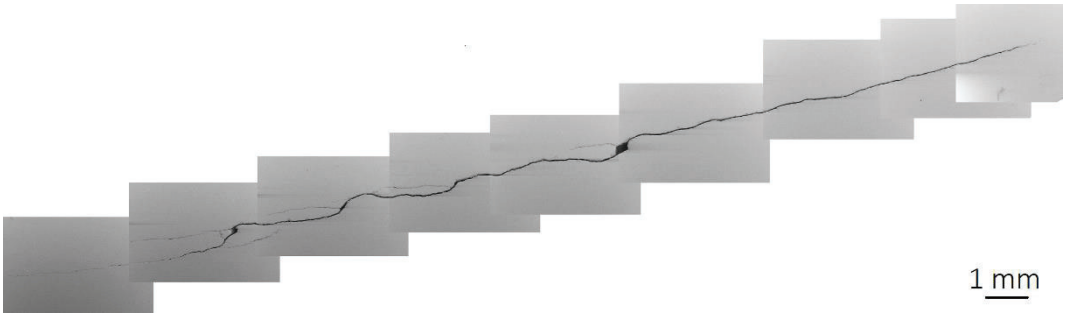

Figure 14. SEM micrographs of sections from a squat, showing crack branching in transverse sections, not distinguishable by geometric reconstruction.

Finally, in Paper 1, X-ray tomography was done on a squat crack network, in order to detect features, such as crack branching, and overall crack geometry and crack face topography. The results are shown in Figure 15. From this study, it was concluded that the different methods are complementary, and observations made using one method can supplement and explain the deficiencies of other methods.

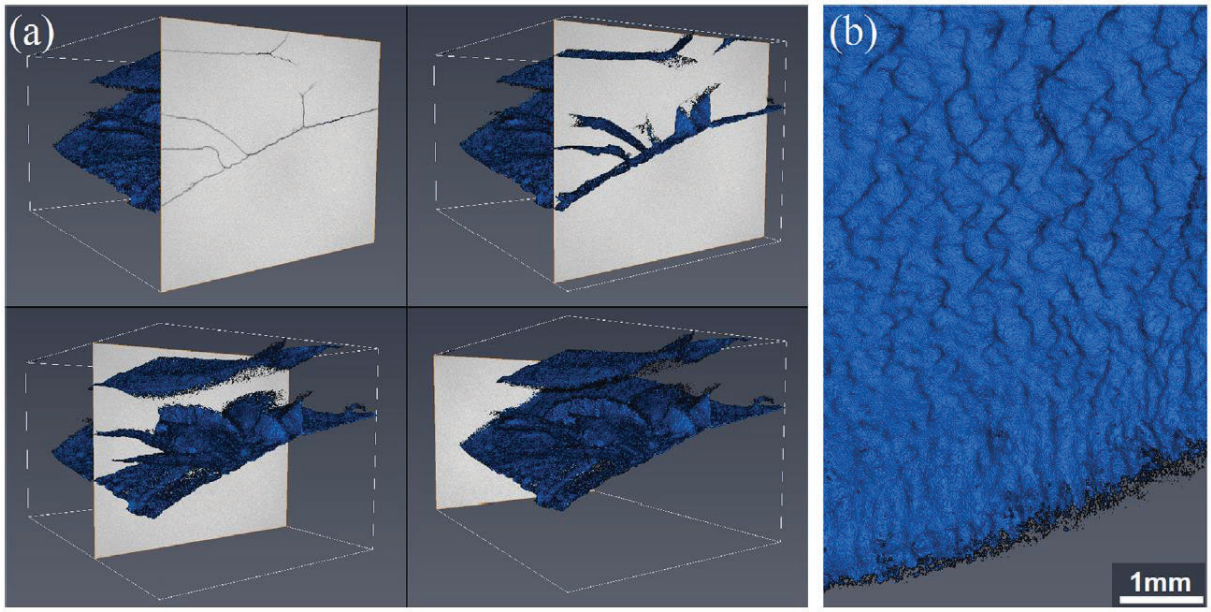

Figure 15. (a) 3D representation of the crack network in blue. Four sections through the reconstructed volume illustrate how the images in [[Fig. 9 in [59]] are taken. (b) Overhead view showing crack ridges.[59]

Plastic deformation

Further metallographic investigation of rail sections taken from the field allowed for a closer look at the area within and around the crack, providing better insight into the mechanisms involved in crack propagation, such as plastic deformation and possible thermal damage. It was found that plastic deformation had occurred, mostly around the surfaces of the crack (e.g. Figure 16). However, it is not seen along the entire length in the transverse sections. Around the crack opening, the deformation of pearlite grains was clearly seen, shown in Figure 16. Realignment of grains was apparent at certain areas along the crack, however, some areas seem unaffected. This suggests the crack did not grow following the severely deformed microstructure, and that other parameters affect the growth path through the bulk of the material.

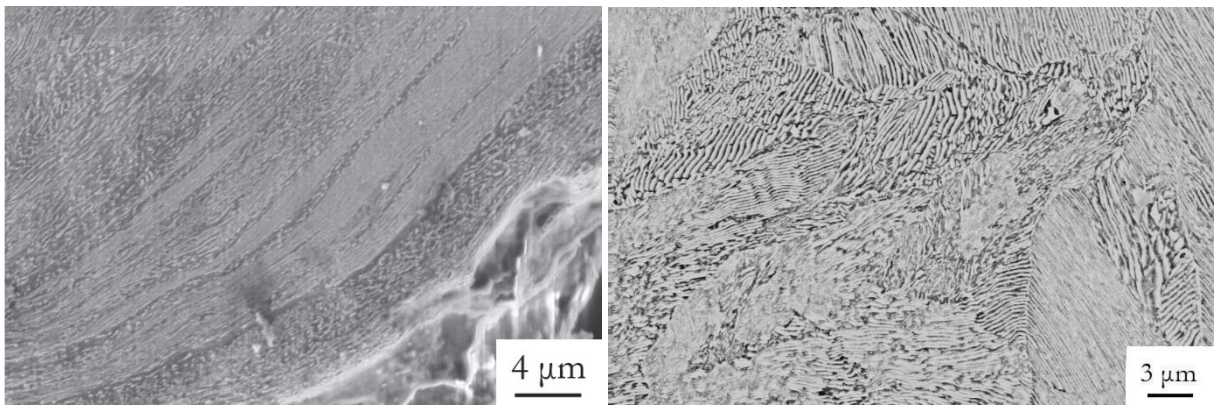

Figure 16. Deformation of pearlite colonies along the edge of the crack (left), compared to the bulk material (right).

Part 2: Effect of thermally induced defects on crack formation (Papers 2 and 3 and unpublished)

Secondly, investigation of crack initiation from thermally damaged surface spots was carried out via strain-controlled LCF experiments using a MTS 809 servo-hydraulic test machine. The effect of initial thermal damage (small martensite spot on test bars) on fatigue crack initiation was examined and evaluated relative to smooth specimens. Comparisons between the WELs observed in field samples and those produced artificially on test bars and railheads were made regarding microstructure and residual stresses. The presence of initial thermal damage was found to slightly reduce fatigue life.

Thermal damage

Thermal damage is often found on rails and wheels, and initial inspection of a rail section taken from the field showed quite severe spalling occurring on the surface, in addition to a large thermally damaged strip, the origination of which cannot be determined (Figure 17). The surface was cleaned and etched using Nital in order to reveal the presence of a WEL, suggesting some event caused martensite to form as a thin layer on the rail surface. Many small cracks within this layer highlight the brittle nature of the WEL.

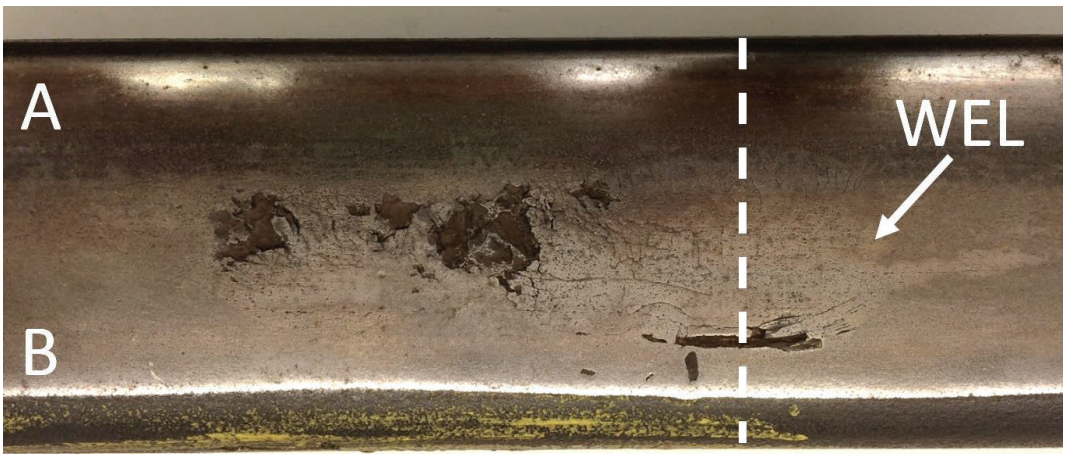

Figure 17. Rail surface after Nital etching: spalling off of large sections is observed in the running band. Section location is shown with a dashed line.

Upon sectioning as shown in Figure 17, the depth of the damage can be more closely examined, including crack patterns and crack depths. The thermal damage is clearly seen in Figure 18. A closer look at the WEL (Figure 18, bottom) shows that there are in fact two different WELs present: a thin (~200 μm) layer appears above a thicker (~550 μm) layer on the surface. The presence of two layers is the result of multiple occurrences of thermal damage (e.g. wheel burns) on the same place. The primary layer exhibits a heat-affected zone, appearing darker just below the secondary layer, which suggests some tempering of the martensite accompanying a second heating event [66]. Furthermore, near the bottom-right corner of Figure 18 deep cracks are present, traveling through the WEL and along the transition between the WEL and bulk material. This could be due to the rolling contact loading occurring between the wheel and rail, affecting the harder and more brittle material within the WEL as well as causing localized strain concentrations beneath the harder layer.

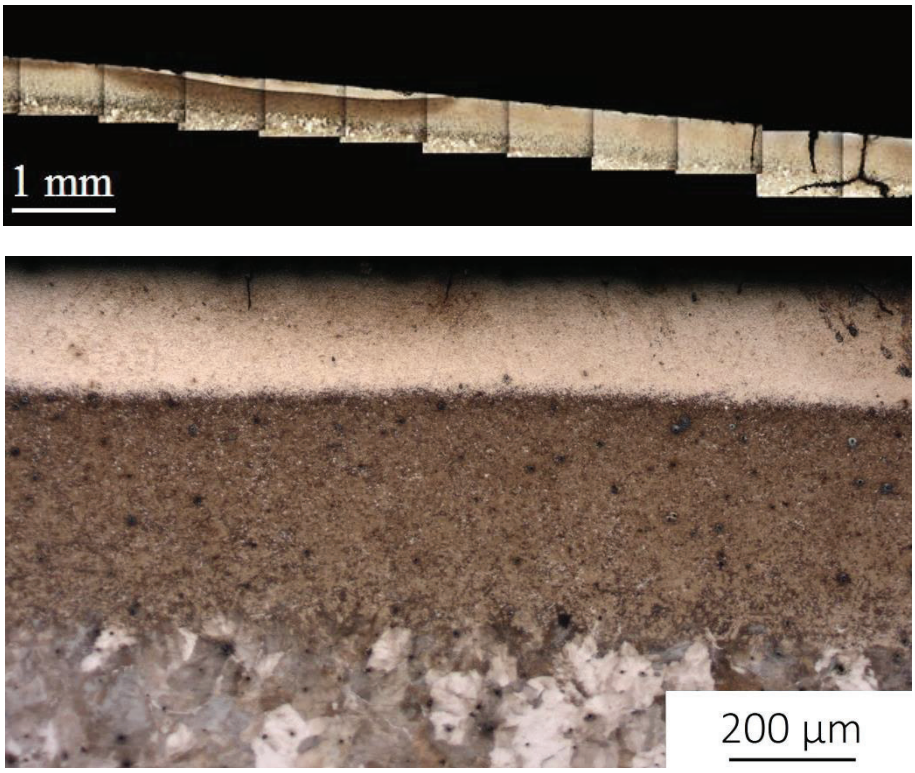

Figure 18. (top) WEL on cross-section from optical microscopy, and (bottom) close-up of double WELs.

Residual stress measurements

The residual stresses measured in the longitudinal and transverse directions around the 6 mm WEL spots on the used and new rail sections are summarized in Figure 20. The test procedure is fully documented in Paper 2. It is seen that comparatively high tensile stresses are present around the WEL spot on both used and new rails, and the stress value approaches zero in the center of the spots. The explanation could be linked to the thermal expansion and plastic deformation of a material volume around the spot upon heating, and volume expansion on martensite formation during subsequent cooling.

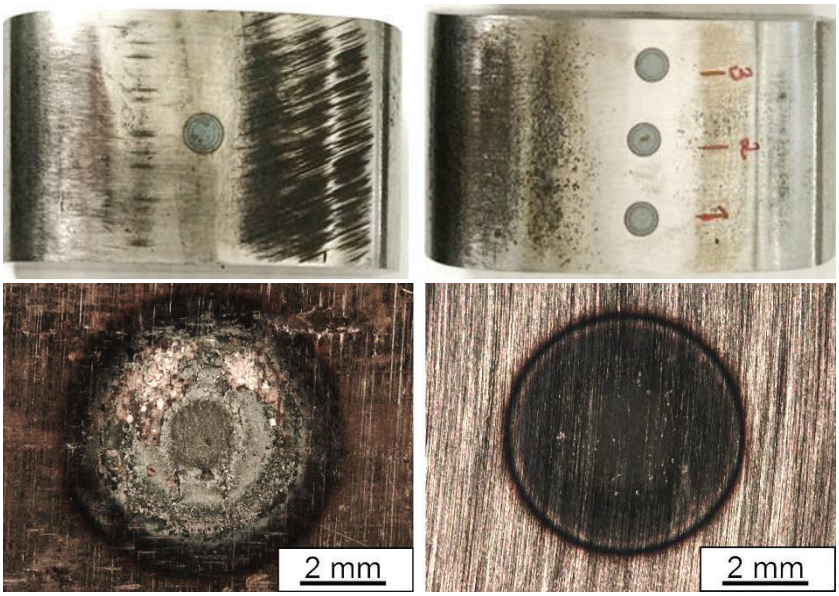

Figure 19. WEL spots on (left) used and (right) new rails.

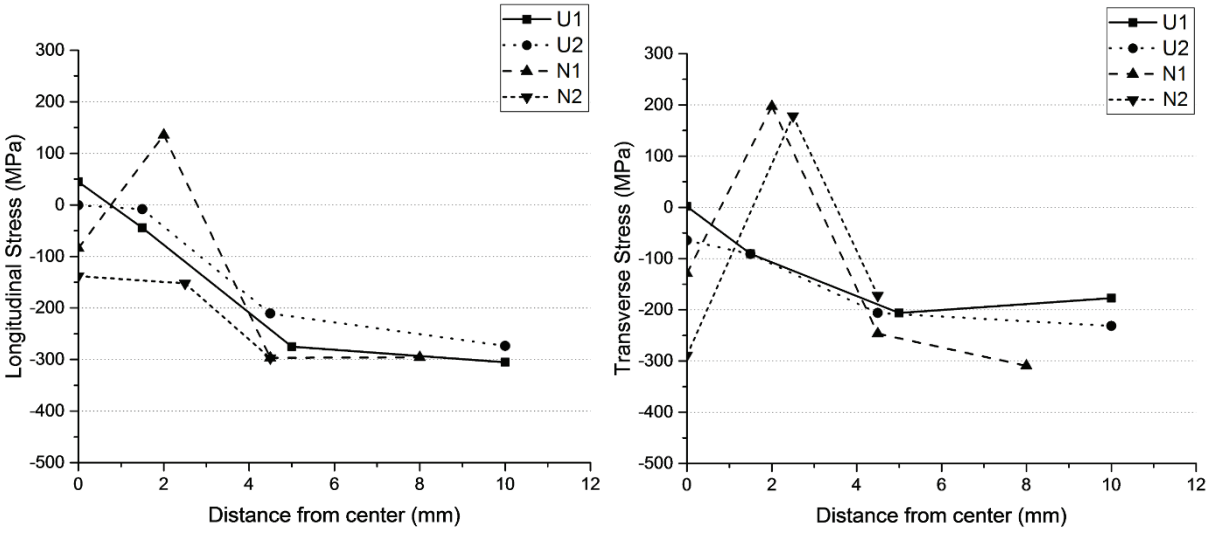

Figure 20. Surface residual stresses around 6-mm WEL spots on used (U1 and U2) and new (N1 and N2) rails.

In Papers 2 and 3 [45], [62], the effect of thermally induced defects on fatigue life and crack formation was investigated with a combination of fatigue testing and characterization of the thermal damage before, during, and after the fatigue tests. Laser-heating experiments (described previously and in Paper 2) were done on smooth test bars in order to create a small martensite spot, mimicking WEL found in the field. These spots were examined using optical and stereo microscopy, and residual stresses measurements were done. The results from the fatigue tests are summarized in Figure 21.

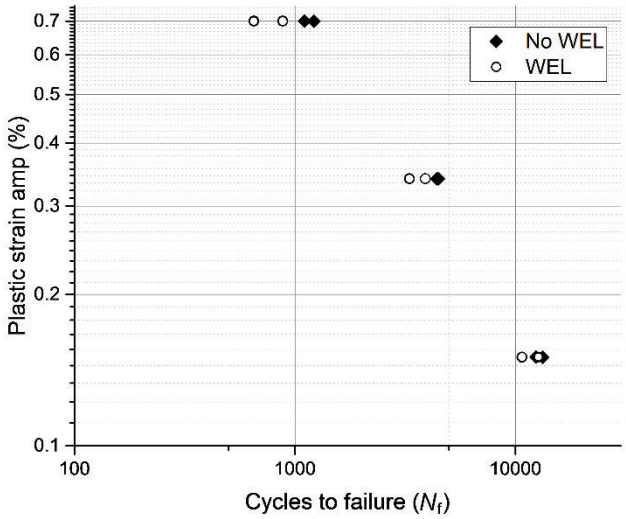

Figure 21. Coffin-Manson plot for uniaxial fatigue tests performed on smooth (diamonds) and thermally damaged (circles) test bars.[45]

The presence of the WEL spot reduced fatigue life in all but one tests, and it was seen that in test bars with thermal damage, the crack was at or near the WEL spot. In order to investigate further the effect of the thermal damage on the crack initiation, digital image correlation (DIC) equipment was set up for one fatigue test. Using this equipment, the deformation on the surface of the test bar can be measured in real time, and the strains are calculated. It could be clearly seen that within the first cycles already, the strains accumulate at the top and bottom of the WEL, in the loading direction. One crack then becomes dominant, and the strains continue to accumulate until failure occurs (Figure 22).

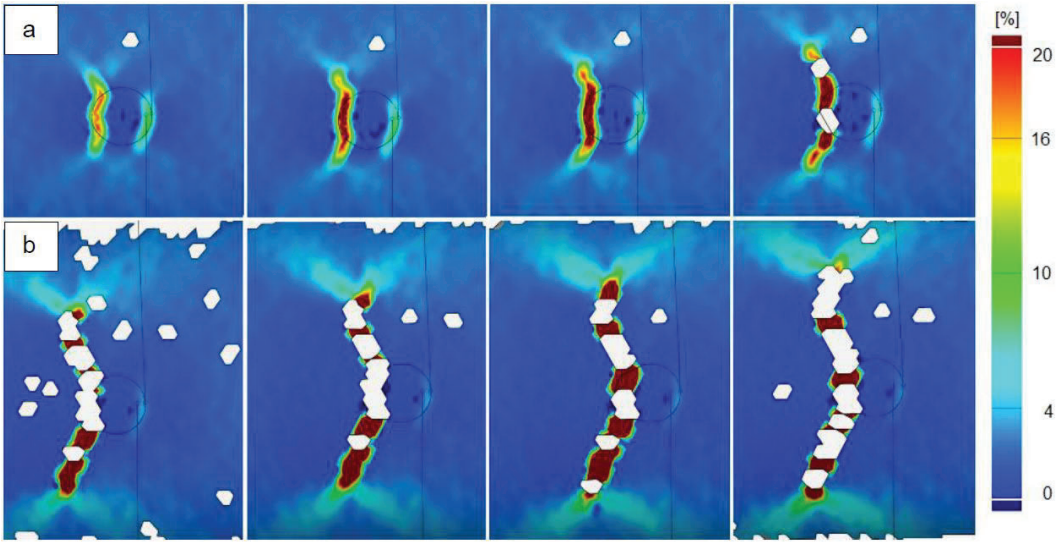

Figure 22. Strain evolution around the WEL during LCF fatigue test (loading in horizontal direction) a) in early stages, and b) during the final 4 cycles before failure, obtained from DIC.[45]

Upon closer examination of the failed test bars with thermal damage, it was found that in some instances, the dominant crack was growing through the WEL (Figure 23), whereas in other test bars, the crack followed the interface between the WEL and the bulk pearlitic material. In addition to metallographic sectioning, X-ray tomography was used to view the crack network in three-dimensions inside the test bar. This method is non-destructive, as previously described, and allowed for the entire crack network to be seen following the WEL on the surface, then propagating in a plane perpendicular to the loading direction, typical of mode I crack propagation. No crack branches were observed.

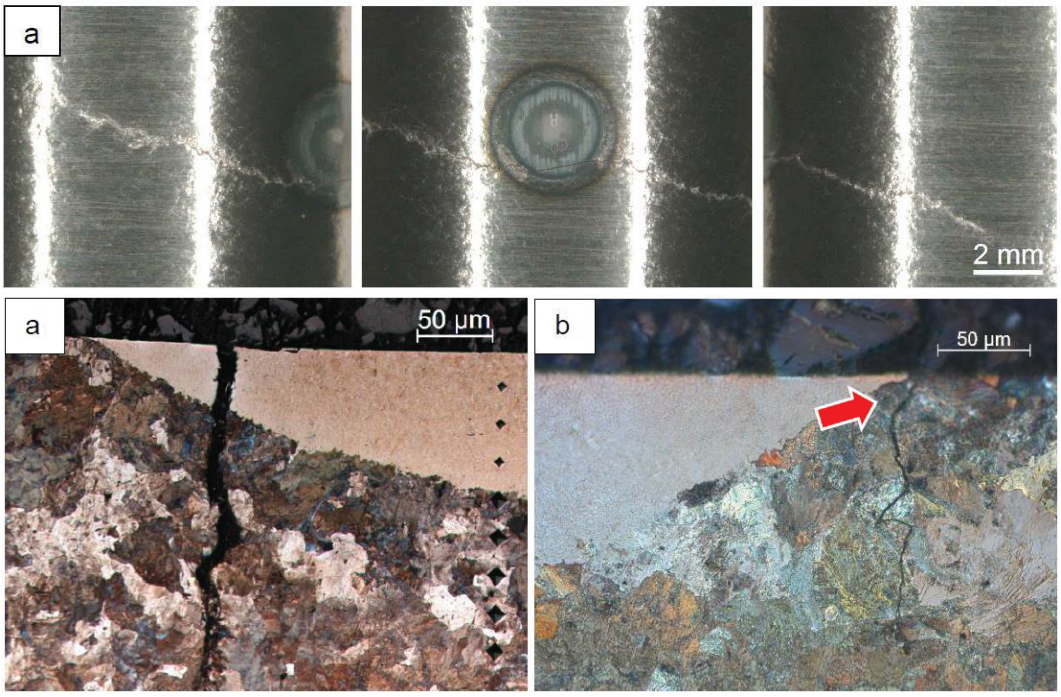

Figure 23. (a) Crack propagation through WEL on fatigue test bar.[45] (b) The crack initiated in the WEL and propagated down into the bulk material. (c) A small crack initiated at the edge of the WEL (polarized light in optical microscope).[62]

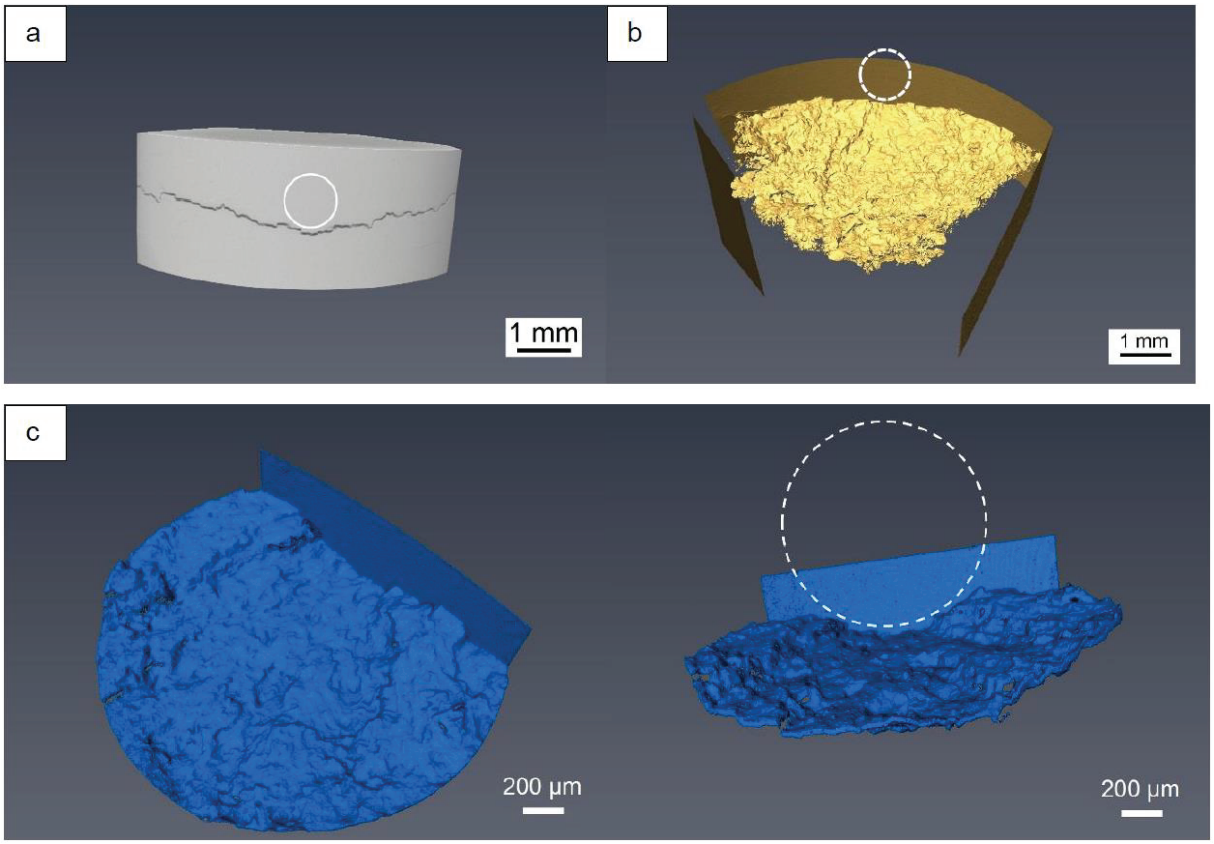

Figure 24. (a) X-ray tomograph of the extent of the crack on the surface of the test bar, (b) overall scan of the crack network within the test bar, and (c) detail scan near the WEL, showing the crack following the bottom of the WEL spot (dashed line represents the approximated location of the WEL spot). [45]

Observation of the fracture surfaces for all tests (with same strain amplitude) revealed that the initial thermal damage does not affect the crack propagation, but only the crack initiation. That is, the WEL spot acts as a stress-raiser during the uniaxial loading, and leads to crack formation earlier, however the remainder of the fatigue life is not affected by the thin WEL spot. The effect of different factors on crack propagation was studied in the next part of the project.

Part 3: Effect of crack face friction on crack propagation (Paper 4 and unpublished)

In addition to the friction which exists in the wheel-rail contact during railway operation, there is an additional friction which is important to the study of crack propagation: crack face friction. That is, the friction between the faces of a crack. The tribology in this area is difficult to study and to measure, due to the very tightly closed cracks in field and during experiments. In order to study the crack face friction independent of crack propagation experiments, a series of tests was designed in which the influence of different factors on the coefficient of friction would be determined. A full description of the experiments and the test specimen can be found in the Paper 4 [63].

Residues

One factor which is thought to influence the friction between crack faces, and subsequently crack propagation, is the presence of third body materials, such as residues within the cracks. A squat was cross-sectioned longitudinally (parallel to the traffic direction) and examined for the presence of residues (see Figure 25). Through scanning electron microscopy and energy-dispersive X-ray spectroscopy (EDX), it was found that the residues have an increased oxygen content compared with the bulk. However, elongated pearlite grains are observed around the crack faces and even within the residues (Figure 26 b and d). This suggests that the residues result in part from the crack propagation that shears bulk material that has broken off from the crack edges [67].

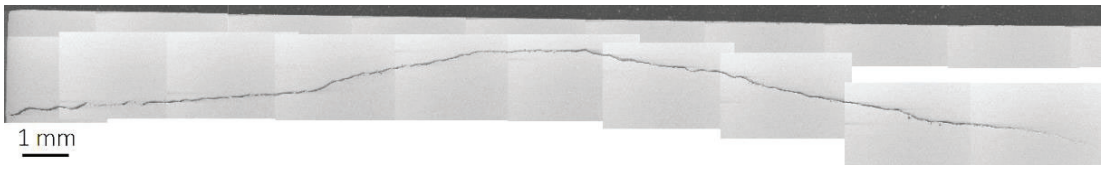

Figure 25. Longitudinal cross-section of squat.

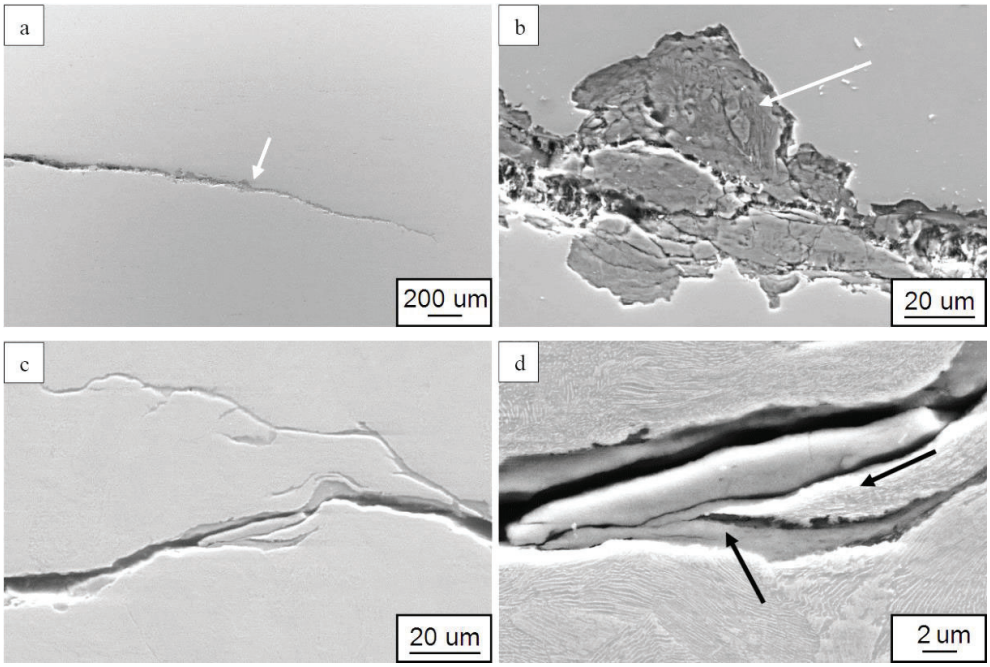

Figure 26. SEM image showing residues in cracks. a) Dark grey material near crack tip are residues, b) close-up showing deformed microstructure within the residues, c) and d) are from a transverse section of the rail.

Friction experiments

The friction experiments lead to the result that although there appears to be a directional dependence on the measures coefficient of friction, the variation is reduced with increasing normal force. Figure 27 shows the coefficient of friction as a function of time in three experiments with varying normal force. Although the average friction coefficient remains approximately the same for all experiments, the variation during each cycle is reduced with increasing normal force.

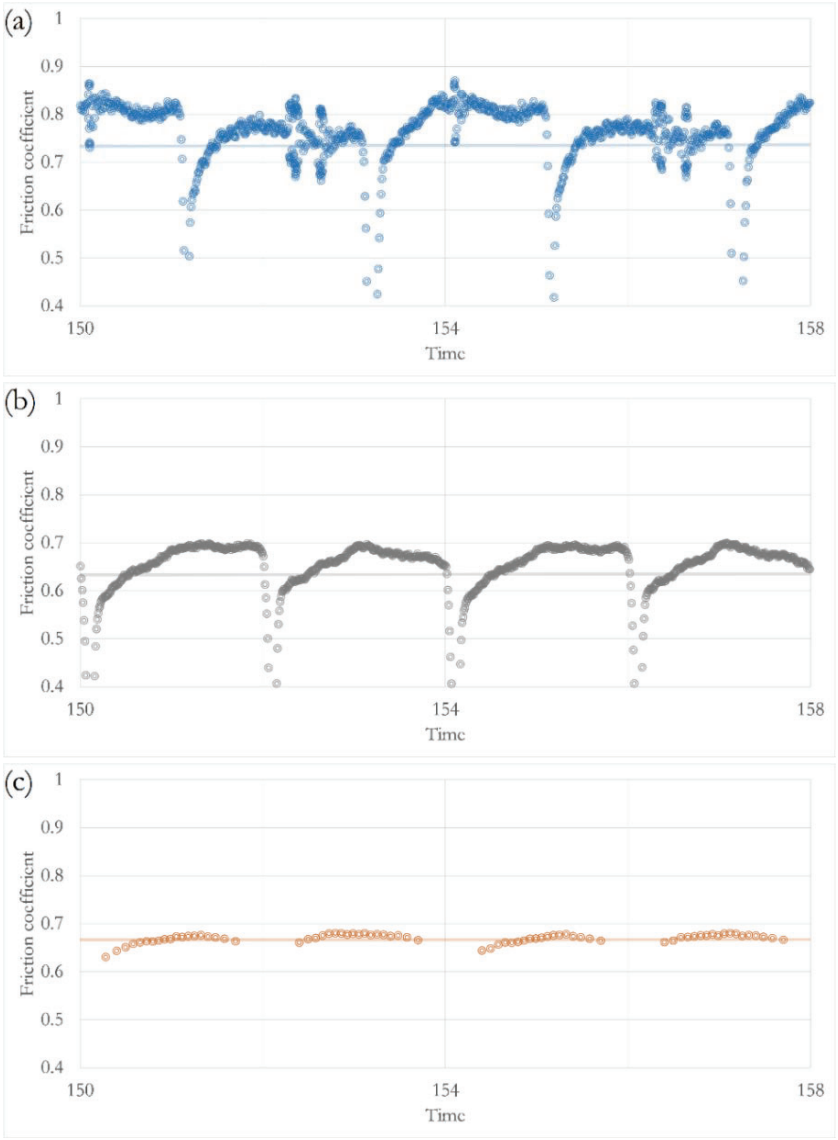

Figure 27. Friction coefficient with respect to time for different normal forces equivalent to: (a) 17.5 MPa, (b) 70 MPa, and (c) 140 MPa (Tests F1, F2, and F3, respectively). The difference between the maximum and minimum values decreases with increasing normal force.

The most significant findings from the friction experiments were related to the deformation of the surfaces, and the effect of adding water to the contact. The ridges on the deformed surfaces are similar to those seen on the squat crack faces, Figure 28. The addition of water in the contact between the two surfaces reduces the coefficient of friction, from approximately 0.63 to 0.38. The reduction of the friction coefficient is accompanied by a reduction in deformation and wear on the surfaces, as seen in Figure 29.

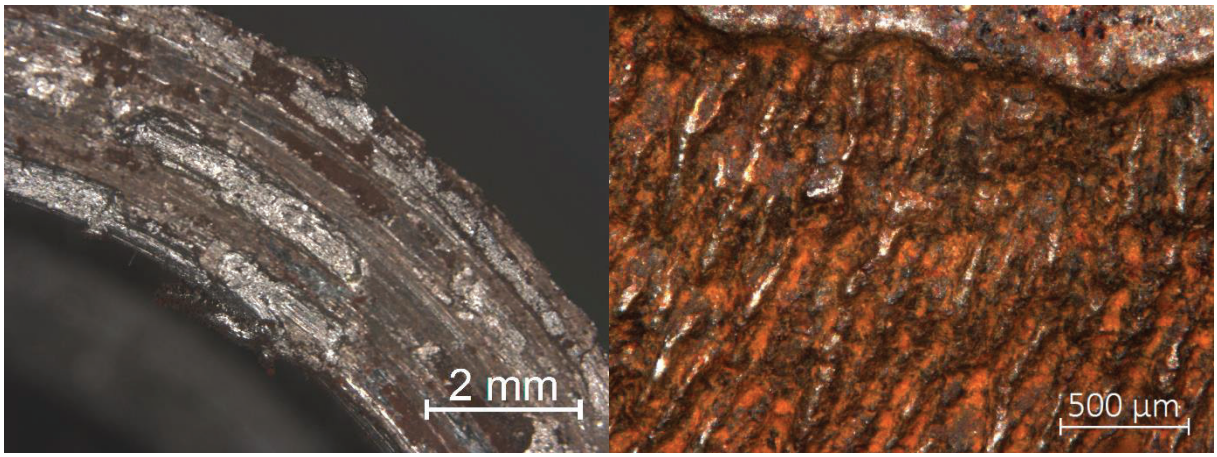

Figure 28. Surface of test bar after friction experiments (left), resembling detail of ridges on squat crack face (right). Modified from [63]

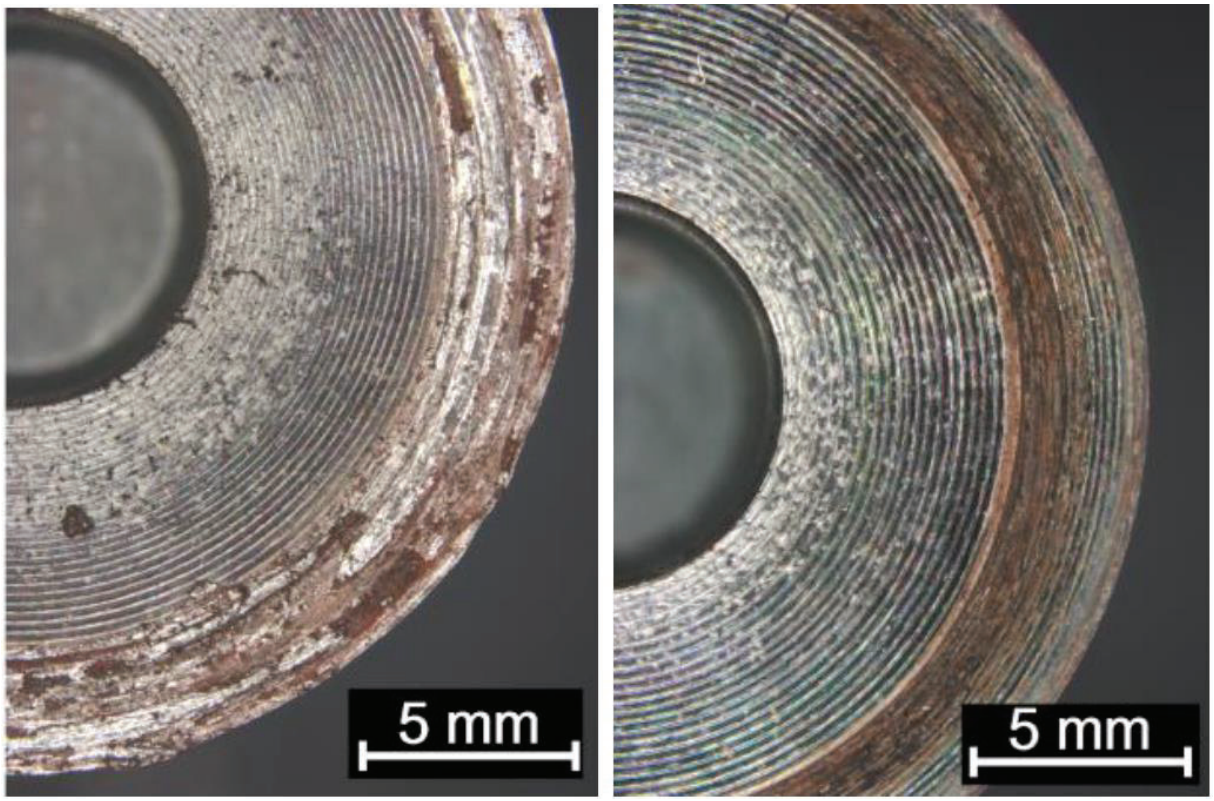

Figure 29. Surfaces of test bar after testing in (left) dry and (right) wet conditions. The more pronounced deformation and wear in the dry conditions is apparent and a reflection of the larger coefficients of frictions calculated. The periphery of the contact surface in the wet tests remains in original condition, while the inner radius is worn and corroded. [63]

Part 4: Mechanical and thermal damage in wheel steel (Paper 5 and unpublished)

The problem with damage and associated failures in railway components can be separated into two main categories: mechanical damage and thermal damage. Although both interplay in reality, for the simplicity of the topic, we will address both as separate issues. In terms of mechanical damage, the thesis has investigated rolling contact fatigue cracks in rails, specifically squats and squat-type defects, which have been the focus of Paper 1, as well as much of the research in recent years. Thermal damage has been studied as, firstly, an initiation site for cracks, in the form of white etching layers (Papers 2 and 3), and secondly, related to residual strains and residual stresses within the bulk material, to be discussed in this section.

Mechanical damage

A detailed investigation was carried out on wheels removed from operation and has been reported in [68]. The RCF damage was studied with stereo and optical microscopy to establish crack morphology and depth. RCF damage is classified according to Figure 30, where RCF1 corresponds to wheel/rail contact on the inner rail in curves, RCF2 on contact on the outer rail in curves, and RCF3 to operations on tangent track and in shallow curves. The results from the investigation show typical properties and RCF damage of used wheels.

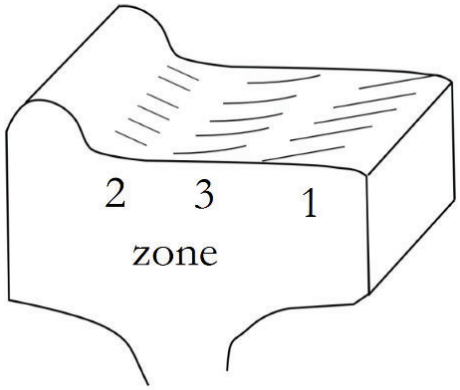

Figure 30. Definition of RCF1, 2 and 3 zones following [69]. Modified from [70].

Macro photographs from visual inspection show RCF1 and RCF3 damage bands spread around the entire circumference (Figure 31). After the first overall examination, the surfaces of the wheels were etched using Nital, but no clear signs of martensite patches became apparent. This, in combination with the continuous damage, speaks against thermal initiation of the cracks, e.g. at small wheel flats or more serious skid patches. It should be noted that this does not imply that thermal loading had no influence on the damage formation, since it has been shown that even moderate thermal loads may have a detrimental influence on the wheel material [71]. However, no high temperature events, i.e. large-scale sliding of the wheel on the rail, have been involved in the formation of damage.

A segment with significant damage was further investigated by stereo and optical microscopy. The typical appearance of RCF1 cracks is shown in Figure 32, with cracks extending up to 0.5 mm into the wheel, growing at small angles, and repeated along the surface of the longitudinal section. In the transverse section, Figure 33, the RCF1 zone lies around the 100 mm mark; however the cracks are not clearly seen in the magnification used. The scratches which can be seen are from sample preparation.

The RCF3 zone in Figure 32 showed a different crack morphology; the cracks are much deeper than in the RCF1 zone, extending to a depth of more than 7 mm, and crack branching is present. It is seen that the RCF3 cracks in the transverse section (Figure 33) are very pronounced, and the majority of the network

extends approximately 2 mm into the wheel. Furthermore, a crack is seen at a depth of 5 mm from the surface. This confirms that dominant cracks extend to at least to this depth, as seen in the longitudinal section, since each section only represents a 2-dimensional image of the whole crack network. It can be concluded that the main damage mechanism is RCF3.

Figure 31. Wheel treads with RCF1 and RCF3 damage bands.

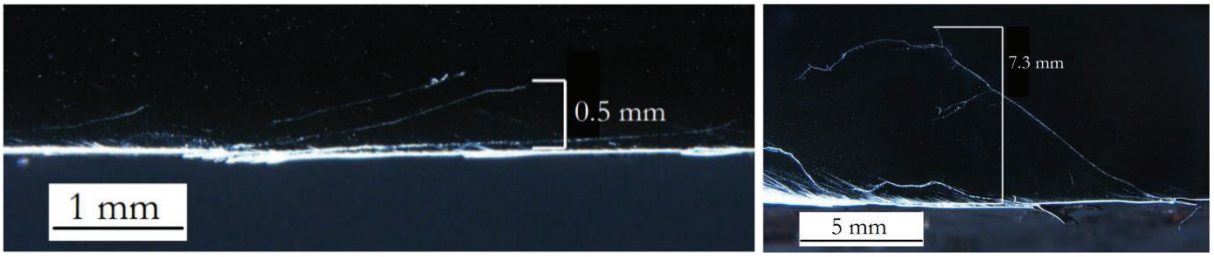

Figure 32. (left) RCF 1 and (right) RCF3 longitudinal sections.

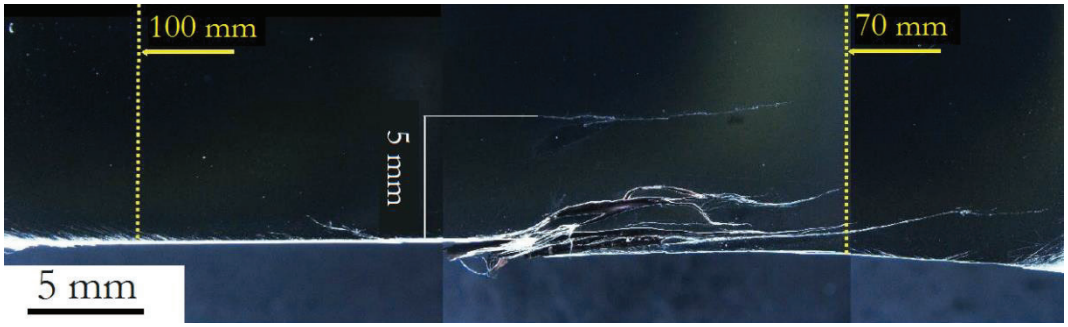

Figure 33. Transverse section through the RCF1 and RCF3 zones. Dotted lines indicate distances of 70 mm and 100 mm from the flange side. These distances correspond to the longitudinal sections of RCF3 and RCF1, respectively.

The sections were further examined by optical microscopy, to investigate in particular the occurrence of plastic deformation and thermal damage. No thermal damage was found in any of the sections, however plastic deformation was observed around the cracks. Figure 34 shows an example of plastic deformation in the vicinity of a RCF3 zone crack; the deformation and grain elongation that appears along the surface of the wheel (bottom) and the faces of the crack can be clearly seen in the magnified view. The damage pattern is typical for surface initiated rolling contact fatigue and there were no signs of severe thermal damage.

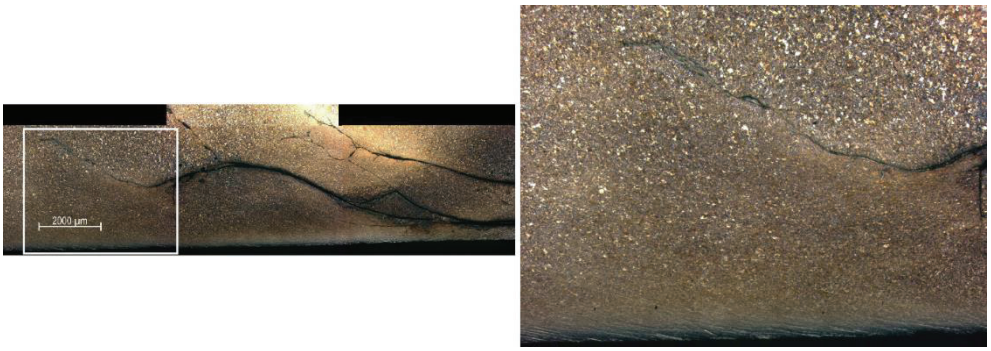

Figure 34. (Left) Example of cracks in longitudinal section through the RCF3 zone. (Right) Magnified view showing plastic deformation around crack and along the wheel surface (bottom of micrograph).

Investigation of misorientation and strains

The effect of thermal damage in the form of white etching layers on the crack initiation has been investigated by fatigue experiments using rail steel. However, in the project, we have also observed the effect of temperature on the bulk material, which is, looking at the material below the surface which has been heated due to one of several possible reasons: braking, acceleration, wheel slip, etc. The temperatures in these circumstances can reach austenization temperature, as addressed previously, while the temperature in the wheel tread can rise up to 550 °C during freight operation [49]. The effects of this on mechanical properties had been investigated within several CHARMEC projects, as well as by different researchers. The focus of the work done within this thesis has been on the effect of annealing on the misorientation and residual strains within ferrite grains in R8T steel, using advanced characterization methods (EBSD and DAXM).

Both methods offer advantages, and a combination of them allows for a good understanding of the behaviour of the material. Using EBSD, it is possible to index the ferrite grains and the pearlitic colonies, and to obtain information from the surface of the sample about local misorientation. The orientation variation in the pearlite colonies is larger than that in the ferrite grains, due to the formation of the lamellar structure of the pearlite. With increasing temperature and annealing time, the misorientation in the ferrite grains decreases. An example of the obtained maps is shown in Figure 35, for the sample annealed at 500 °C for 4h.

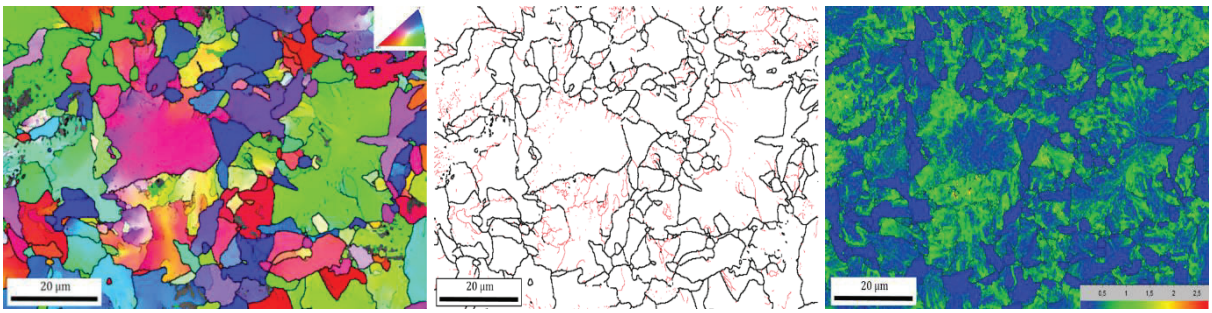

Figure 35. Maps from EBSD (R8T sample annealed at 500 °C for 4h). Modified from Paper 5. [72]

Using DAXM, we measure along a 45° plane into the sample (that is, we look into the sample). In addition to misorientation information, we can also obtain information on the relative strain in selected grains. Due to the high brightness/intensity of the beam coming from the synchrotron source, a higher resolution is obtained. It was found that the samples annealed at 300 °C and 500 °C are very similar in terms of misorientation, and there is little difference in the local misorientation in the two samples as well as the

average misorientation. The maps for the sample annealed at 500 °C is shown in Figure 36. The legend corresponds to the distribution of local misorientation angles in the KAM map. There is limited indexing using this method, and due to the larger orientation variations within pearlite colonies that cannot always be indexed, and we are left with a large portion of unresolved points. It was observed, however, that when the sample is fully spheroidized a larger portion of the plane is indexed. Annealing at 690 °C for 96h results in a fully spheroidized microstructure, as shown in Figure 6b. Lower local misorientation is observed after full spheroidization, and more ferrite grains are indexed, as can be seen from the IPF and KAM maps in Figure 37. This suggests that the method works better when indexing the microstructure without cementite plates, since the cementite is no longer present as lamellas within the pearlite grains, but rather as large spheres or carbides within a ferrite matrix.

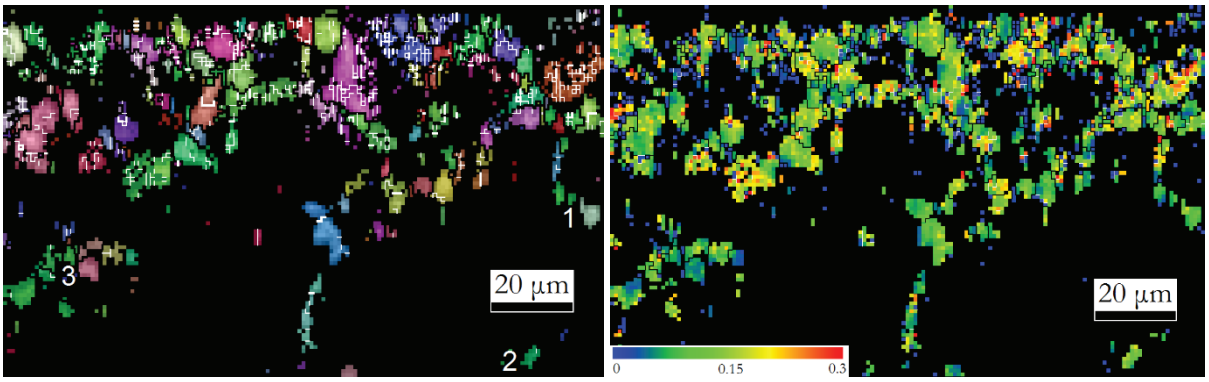

Figure 36. R8T sample annealed at 500 °C for 4h. (a) IPF, and (b) KAM showing misorientation below 0.3° within the grains. (Sample surface at top)

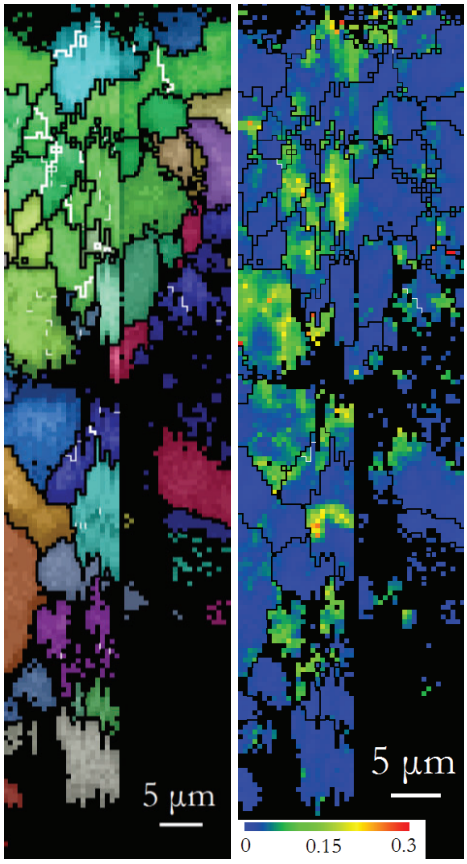

Figure 37. SEM micrograph of R8T sample annealed at 690 °C for 96h, and corresponding IPF and KAM maps showing better indexing when cementite is spheroidized versus lamellar. (Sample surface at top)

Moreover, the use of monochromatic beams allows for the determination of relative strain within single ferrite grains using DAXM. Figure 38 shows the grains (numbered in Figure 36) in which strains were measured based on calculated strain-free lattice parameters for the sample annealed at 500 °C for 4 hours. It can be seen that the range of residual strains, 3 x 10^{-4} (-2 to 0.7 10^{-4}), is nearly zero, showing that temperature releases most residual strains within single grains, and the variation is decreased with increased annealing temperature.

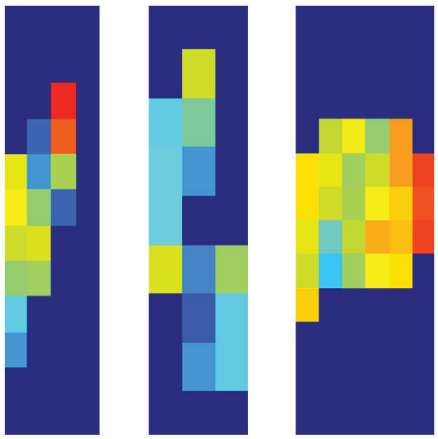

Strain (x10^{4})	Grain 1	Grain 2	Grain 3
Min.	-0.565	-0.650	-2.38
Max.	0.683	0.157	0.00572
Range	1.25	0.807	2.44

Figure 38. Range of strains measured in 3 ferrite grains in the sample annealed at 500 °C for 4h. The grains are numbered in Figure 36.

Conclusions

The aim of the project was to properly characterize mechanical and thermal defects in railway components, and evaluate their effects on crack initiation and propagation, and on mechanical properties. This has been explored in some different steps and through different methods, and it has been found that many factors affect these phenomena. The work was separated into three main objectives. The first is to properly describe the 3D network of RCF defects in railway rails and wheels using several characterization techniques. The second is to study the influence of different factors on crack initiation and propagation through fatigue tests, including friction experiments. The third is to investigate the effect of annealing on the microstructure and bulk properties of wheel steel.

A good understanding and accurate description of crack morphology and thermal defects as crack initiators, have been important elements to investigate relevant parameters and provide input for models. Additional experiments in different climatic conditions (temperature and humidity) are important to expand the results. Squat crack networks were described using several methods, detection limits of each technique have been clarified, and it was concluded that using a combination of several methods the network can be accurately described on many scales.

Extensive characterization of damage found in field is used to design experiments. Different factors influencing the crack growth are investigated using laboratory tests, e.g. fatigue and friction experiments. Well-defined WELs similar to those found in field were produced using laser welding equipment, and the effect of these WEL spots on crack initiation and fatigue life has been shown. The WELs reduce fatigue life by providing a crack initiation site; both by stress and strain concentration and by decreasing ductility. Additionally, it was observed that failure occurs at the WEL in all cases except one, with the crack initiating in the martensite and growing outwards.

Furthermore, a method to examine crack face friction has been identified, and using this method, similar crack face features to those observed in cracks from field are created in the lab. The results from the friction experiments can be used as input towards crack propagation experiments.

Finally, the effect of thermal damage on bulk properties was also investigated using EBSD and DAXM. It was found that the variation in local misorientation and residual strains decreases with increasing annealing temperature and time.

References

[1] Trafikanalys, "Rail traffic accidents 2014," 2015.

[2] H. Schwarz, "Improving the sustainability of transport – The rail sector as a case study," New York, 2011.

[3] R. Clark, "Rail flaw detection: overview and needs for future developments," *NDT E Int.*, vol. 37, no. 2, pp. 111–118, 2004.

[4] Office of Rail Regulation, "Train Derailment at Hatfield: A Final Report by the Independent Investigation Board," 2006.

[5] Railways Archive, "Accident at Hatfield on 17th October 2000." [Online]. Available: http://www.railwaysarchive.co.uk/eventsummary.php?eventID=143. [Accessed: 07-Apr-2016].

[6] M. Steenbergen Dollevoet, R., "On the mechanism of squat formation on train rails- Part I: Origination," *Int. J. Fatigue*, vol. 47, pp. 361–372.

[7] M. Steenbergen Dollevoet, R., "On the mechanism of squat formation on train rails- Part II: Growth," *Int. J. Fatigue*, vol. 47, pp. 373–381.

[8] S. L. Grassie, D. I. Fletcher, E. A. Gallardo-Hernandez, and P. Summers, "'Squats' and 'studs' in rails: similarities and differences," *Proc. Inst. Mech. Eng. Part F J. Rail Rapid Transit*, vol. 226, no. 3, pp. 243–256, 2011.

[9] S. Bogdanski, M. Olzak, and J. Stupnicki, "Numerical stress analysis of rail rolling contact fatigue cracks," *Wear*, vol. 191, no. 1–2, pp. 14–24, 1996.

[10] J. E. Garnham and J. H. Beynon, "The early detection of rolling-sliding contact fatigue cracks," *Wear*, vol. 144, no. 1–2, pp. 103–116, 1991.

[11] S. L. Grassie, "Squats and squat-type defects in rails: the understanding to date," *J. Rail Rapid Transit*, vol. 226, pp. 235–242, 2011.

[12] A. Ekberg, B. Åkesson, and E. Kabo, "Wheel/rail rolling contact fatigue – Probe, predict, prevent," *Wear*, vol. 314, no. 1–2, pp. 2–12, 2014.

[13] Z. Li, X. Zhao, C. Esveld, R. Dollevoet, and M. Molodova, "An investigation into the causes of squats- Correlation analysis and numerical modeling," *Wear*, vol. 265, pp. 1349–1355, 2008.

[14] H. M. Tournay and J. M. Mulder, "The transition from the wear to the stress regime," *Wear*, vol. 191, no. 1–2, pp. 107–112, 1996.

[15] C. Bernsteiner, G. Müller, A. Meierhofer, K. Six, D. Künstner, and P. Dietmaier, "Development of white etching layers on rails : simulations and experiments," vol. 367, pp. 116–122, 2016.

[16] W. Österle Rooch, H., Pyzalla, A., Wang, L., "Investigation of white etching layers on rails by optical microscopy, electron microscopy, X-ray and synchotron X-ray diffraction," *Mater. Sci. Eng. A*, vol. 303, pp. 150–157, 2001.

[17] R. I. Carroll and J. H. Beynon, "Rolling contact fatigue of white etching layer: Part 1 Crack morphology," *Wear*, vol. 262, pp. 1253–1266, 2007.

[18] R. I. Carroll and J. H. Beynon, "Rolling contact fatigue of white etching layer: Part 2 Numerical results," *Wear*, vol. 262, pp. 1267–1273.

[19] S. Pal, W. Daniel, and M. Farjoo, "Early stages of rail squat formation and the role of a white etching layer," *Int. J. Fatigue*, vol. 52, pp. 144–156, 2013.

[20] R. Pohl Erhard, A., Montag, H.-J., Thomas, H.-M., Wüstenberg, H., "NDT techniques for railroad wheel and gauge corner inspection," *NDT&E Int.*, vol. 37, pp. 89–94, 2004.

[21] R. Pohl Krull, R., Meierhofer, R., "A new Eddy current instrument in a grinding train," *ECNDT*. 2006.

[22] M. P. Papaelias Roberts, C., Lewis, C.L., "A review on non-destructive evaluation of rails: state-of-the-art and future developments," *J. Rail Rapid Transit*, pp. 367–384, 2008.

[23] A. F. Bower and K. L. Johnson, "Plastic flow and shakedown of the rail surface in repeated wheel-rail contact," *Wear*, vol. 144, 1991.

[24] A. Ekberg and E. Kabo, "Fatigue of railway wheels and rails under rolling contact and thermal loading - an overview," *Wear*, vol. 258, pp. 1288–1300, 2005.

[25] W. R. Tyfour, J. H. Beynon, and A. Kapoor, "Deterioration of rolling contact fatigue life of pearlitic rail steel due to dry-wet rolling-sliding line contact," *Wear*, vol. 197, no. 1–2, pp. 255–265, 1996.

[26] A. Hohenwarter and R. Pippan, "Fracture and fracture toughness of nanopolycrystalline metals produced by severe plastic deformation Subject Areas :," *Philos. Trans. R. Soc. A Math. Phys. Eng. Sci.*, vol. 373, no. 2038, p. Article number 20140366, 2015.

[27] C. Jessop, "Damage and thermally induced defects in railway materials," 2017.

[28] Z. Li, "Squats on railway rails," *Wheel-rail interface handbook*, no. 13. pp. 409–436, 2009.

[29] S. Kaewunruen, "Identification and prioritization of rail squat defects in the field using rail magnetisation technology," vol. 9437, p. 94371H, 2015.

[30] J. Smulder, "Management and research tackle rolling contact fatigue," *Railway Gazatte International*, pp. 439–442, 2003.

[31] S. L. Grassie, "Studs and squats : The evolving story," vol. 367, pp. 194–199, 2016.

[32] H. C. Eden, J. E. Garnham, and C. L. Davis, "Influential microstructural changes on rolling contact fatigue crack initiation in pearlitic rail steels," *Mater. Sci. Technol.*, vol. 21, no. 6, pp. 623–629, 2005.

[33] Y. Jin, F. Aoki, M. Ishida, and A. Namura, "Investigation and Analysis of the Occurence of Rail Head Checks," *Int. J. Railw.*, vol. 2, no. 2, pp. 43–49, 2009.

[34] S. L. Wong, P. E. Bold, M. W. Brown, and R. J. Allen, "A branch criterion for shallow angled rolling contact fatigue cracks in rails," *Wear*, vol. 191, pp. 45–53, 1996.

[35] S. L. Grassie, D. I. Fletcher, E. A. Gallardo-Hernandez, and P. Summers, "Studs: a squat-type defect in rails," *J. Rail Rapid Transit*, vol. 226, no. 2011, pp. 243–256.

[36] W. Daniel, S. Pal, and M. Farjoo, "Rail squats: progress in understanding the Australian experience," *J. Rail Rapid Transit*, vol. 227, no. 5, pp. 481–492, 2013.

[37] Z. Li, X. Zhao, and R. Dollevoet, "The determination of a critical size for rail top surface defects to grow into squats," *8th Internationsl Conference on Contact Mechanics and Wear of Rail/Wheel Systems*. Firenze, Italy, pp. 379–388.

[38] Z. Li, X. Zhao, R. Dollevoet, and M. Molodova, "Differential wear and plastic deformation as causes of squat at track local stiffness change with other track short defects," *Veh. Syst. Dyn.*, vol. 46, pp. 237–246.

[39] Z. Li, R. Dollevoet, M. Molodova, and X. Zhao, "Squat growth- Some observations and the validation of numerical predictions," *Wear*, vol. 271, pp. 148–157, 2011.

[40] Z. Li, X. Zhao, C. Esveld, R. Dollevoet, and M. Molodova, "The validation of some numerical predictions on squats growth," *8th International Conference on Contact Mechanics and Wear of Rail/Wheel Systems*. Firenze, Italy, pp. 369–377.

[41] J. Orlich and H. Pietrzeniuk, "Atlas zur Wärmebehandlung der Stähle, Band 4," Düsseldorf: Max-Planck-Institut für Eisenforschung: Verlag Stahleisen M.B.H., 1976, pp. 147–151.

[42] T. Eyre and A. Baxter, "The formation of white layers at rubbing surfaces," *Tribology*, pp. 256–261, 1972.

[43] H. W. Zhang, S. Ohsaki, S. Mitao, M. Ohnuma, and K. Hono, "Microstructural investigation of

white etching layer on pearlite steel rail," *Mater. Sci. Eng. A*, vol. 421, pp. 191–199, 2006.

[44] R. Andersson, J. Ahlström, E. Kabo, F. Larsson, and A. Ekberg, "Numerical investigation of crack initiation in rails and wheels affected by martensite spots," *Int. J. Fatigue*, vol. 114, pp. 238–251, 2018.

[45] C. Jessop, J. Ahlström, C. Persson, and Y. Zhang, "Damage evolution around white etching layer during uniaxial loading," *Fatigue Fract. Eng. Mater. Struct.*, pp. 1–10, 2019.

[46] J. Ahlström, "Residual stresses generated by repeated local heating events – Modelling of possible mechanisms for crack initiation," *Wear*, vol. 366–367, pp. 180–187, 2016.

[47] K. Cvetkovski, J. Ahlström, and B. Karlsson, "Monotonic and cyclic deformation of a high silicon pearlitic wheel steel," *Wear*, vol. 271, pp. 382–387, 2011.

[48] D. Nikas, J. Ahlström, and A. Malakizadi, "Mechanical properties and fatigue behaviour of railway wheel steels as influenced by mechanical and thermal loadings," *Wear*, vol. 366–367, pp. 407–415, 2016.

[49] C. J. Peters and D. Eifler, "Influence of service temperatures on the fatigue behaviour of railway wheel and tyre steels," *Mater. Test.*, vol. 51, no. 11–12, pp. 748–754, 2009.

[50] K. Mädler and M. Bannasch, "Materials used for Wheels on Rolling Stock," in *7th World Congress on Railway Research*, 2014.

[51] D. Nikas and J. Ahlström, "Thermal deterioration of railway wheel steels," 2015.

[52] S. Pal, W. Daniel, A. Atrens, V. Luzin, and M. Kerr, "Role of Residual Stresses in Rail Squat Formation," 2011. [Online]. Available: http://www.ansto.gov.au/ResearchHub/Bragg/CurrentResearch/ScientificHighlights/Roleofresidualstresses/index.htm.

[53] D. A. Skoog, J. F. Holler, and S. R. Crouch, *Principles of Instrumental Analysis*, Sixth Edit. David Harris, 2007.

[54] M. E. Fitzpatrick, A. T. Fry, P. Holdway, F. A. Khadil, J. Shackleton, and L. Suominen, "Determination of Residual Stresses by X-Ray Diffraction- Issue 2," National Physical Laboratory, Teddington, Middlesex, United Kingdom, 2005.

[55] J. R. Griffiths and C. E. Richards, "Fatigue Testing," *Mater. Sci. Eng R*, vol. 11, pp. 305–315, 1973.

[56] N. E. Dowling, *Mechanical Behavior of Materials*, Fourth Edi. Pearson Education, 2013.

[57] H. Hertz, "Über die berührung fester elastischer körper," *J. der reine und Angew. Math.*, vol. 92, pp. 156–171, 1882.

[58] A. Ekberg, E. Kabo, and H. Andersson, "An engineering model for prediction of rolling contact fatigue of railway wheels," *Fatigue Fract. Eng. Mater. Struct.*, vol. 25, pp. 899–910, 2002.

[59] C. Jessop, J. Ahlström, L. Hammar, S. Fæster, and H. K. Danielsen, "3D characterization of rolling contact fatigue crack networks," *Wear*, vol. 366–367, pp. 392–400, 2016.

[60] Y. B. Zhang, T. Andriollo, S. Fæster, W. Liu, J. Hattel, and R. I. Barabash, "Three-dimensional local residual stress and orientation gradients near graphite nodules in ductile cast iron," *Acta Mater.*, vol. 121, pp. 173–180, 2016.

[61] S. Dhar, Y. Zhang, R. Xu, H. K. Danielsen, and D. Juul Jensen, "Synchrotron X-ray measurement of residual strain within the nose of a worn manganese steel railway crossing," *IOP Conf. Ser. Mater. Sci. Eng.*, vol. 219, no. 1, 2017.

[62] C. Jessop and J. Ahlström, "Crack formation in pearlitic rail steel under uniaxial loading: effect of initial thermal damage," in *LCF8 Eighth International Conference on Low Cycle Fatigue*, 2017, pp. 275–280.

[63] C. Jessop and J. Ahlström, "Friction between pearlitic steel surfaces," in *11th Conference on Contact Mechanics*, 2018.

[64] T. M. Inc., "MATLAB and Statistics Toolbox Release 2014b." Natick, Massachusetts, United States, 2014.

[65] S. Simon, A. Saulot, C. Dayot, X. Quost, and Y. Berthier, "Tribological characterization of rail squat defects," *Wear*, vol. 297, pp. 926–942, 2013.

[66] J. Ahlström and B. Karlsson, "Microstructural evaluation and interpretation of the mechanically and thermally affected zone under railway wheel flats," *Wear*, vol. 232, pp. 1–14, 1999.

[67] K. Cvetkovski, J. Ahlström, M. Norell, and C. Persson, "Analysis of wear debris in rolling contact fatigue cracks of pearlitic railway wheels," *Wear*, vol. 314, pp. 51–56, 2014.

[68] C. Jessop, J. Ahlström, and A. Ekberg, "Analysis of cracked wheel," Gothenburg, Sweden, 2015.

[69] R. Deuce, "Wheel tread damage – an elementary guide," 2007.

[70] A. Ekberg and E. Kabo, "Classification of wheel damage," Chalmers University of Technology, Gothenburg, Sweden, 2011.

[71] S. Caprioli and A. Ekberg, "Numerical evaluation of the material response of a railway wheel under thermomechanical braking conditions," *Wear*, vol. 314, no. 1–2, pp. 181–188, 2014.

[72] C. Jessop, Y. B. Zhang, D. Nikas, and J. Ahlström, "Effect of annealing on microstructure and strain in railway wheel steel characterized by electron and synchrotron X-ray diffraction," 2019.